Biomaterials Advances 184 (2026) 214833

Contents lists available at ScienceDirect

Biomaterials Advances

journal homepage: www.journals.elsevier.com/materials-science-and-engineering-c

# Bioengineered baculovirus-derived extracellular vesicles loaded with of γ-carboxylated Gla-rich protein: Dual modulation of inflammation and vascular calcification

Carla Viegas [a,b,*], Simon Pichard [c], Joana Carreira [a], Adélia Ova [a], Nathalie Troffer-Charlier [d], Teresa M. Maia [e,f], Evelina Edelweiss [d], Anjos L. Macedo [g], António Matos [h], Tiago Q. Faria [i,j], Sofia M. Calado [k,l], Carina Monico [a], Simon Devos [e,f], Francis Impens [f,m], Christine Schaeffer-Reiss [n,o], Sarah Cianférani [n,o], Cristina Peixoto [i,j], Arnaud Poterszman [c,d], Dina Simes [a,b]

[a] Centro de Ciências do Mar do Algarve (CCMAR/CIMAR LA), Campus de Gambelas, Universidade do Algarve, 8005-139, Faro, Portugal
[b] GenoGla Diagnostics, CCMAR, Universidade do Algarve, 8005-139, Faro, Portugal
[c] UAR2061 – Biostructure, Institut de Génétique et de Biologie Moléculaire et Cellulaire (IGBMC), 67 404, Illkirch Cedex, France
[d] Institut de Génétique et de Biologie Moléculaire et Cellulaire (IGBMC), CNRS, UMR 7104, Inserm, UMR S 1258, Equipe Labellisée Ligue Contre le Cancer, 67 404, Illkirch, France
[e] VIB Proteomics Core, VIB, 9000, Ghent, Belgium
[f] Department of Biomolecular Medicine, Ghent University, 9000, Ghent, Belgium
[g] UCIBIO, Department of Chemistry, and Associate Laboratory i4HB - Institute for Health and Bioeconomy, FCT-NOVA, Universidade NOVA de Lisboa, 2829-516, Caparica, Portugal
[h] Egas Moniz - School of Health and Science, Caparica, Portugal
[i] iBET - Instituto de Biologia Experimental e Tecnológica, Apartado 12, 2781-901, Oeiras, Portugal
[j] ITQB - Instituto de Tecnologia Química e Biológica António Xavier, Universidade Nova de Lisboa, Av. da República, 2780-157, Oeiras, Portugal
[k] Algarve Biomedical Research Center Institute (ABC-RI), Universidade do Algarve, 8005-139, Faro, Portugal
[l] Faculdade de Ciências e Tecnologia, Universidade dos Açores, 9500-321, Ponta Delgada, Portugal
[m] VIB Center for Medical Biotechnology, VIB, 9000, Ghent, Belgium
[n] Laboratoire de Spectrométrie de Masse Bio-Organique, (LSMBO), IPHC UMR 7178, CNRS, Université de Strasbourg, 67087, Strasbourg, France
[o] Infrastructure Nationale de Protéomique ProFI-UAR2048, 67087, Strasbourg, France

## ARTICLE INFO

*Keywords:*
Extracellular vesicles
Gla-rich protein
γ-carboxylation
Baculovirus expression vector system
Vitamin K–dependent proteins
Inflammation
Calcification

## ABSTRACT

Chronic inflammation and ectopic calcification are interrelated processes driving major chronic inflammatory diseases such as cardiovascular and chronic kidney diseases. Gla-rich protein (GRP), a vitamin K–dependent protein (VKDP) with dual anti-inflammatory and anti-calcific properties, has emerged as a promising therapeutic molecule. However, its biomedical development has been limited by difficulties in producing the γ-carboxylated (cGRP) form and by its poor solubility at physiological pH, constraining formulation and delivery. To address these challenges, we established a baculovirus expression vector system (BEVS) designed to couple GRP post-translational maturation with its secretion in extracellular vesicles (EVs). Co-expression of GRP with γ-glutamyl carboxylase (GGCX), vitamin K epoxide reductase (VKOR), and the convertase Furin enabled efficient γ-carboxylation, propeptide removal, and secretion of mature cGRP. GGCX and VKOR were essential for γ-carboxylation, while Furin mediated propeptide processing. EVs were isolated by differential ultracentrifugation into 30 K and 100 K fractions and characterized by NTA, TEM, Western blot, ELISA, and proteomics. All vesicles displayed physical and molecular features resembling mammalian EVs, including canonical EV markers and distinct proteomic profiles, with GRP, GGCX, VKOR, and Furin preferentially enriched in the 30 K population. Functional assays demonstrated that the resulting EVs associated with human THP-1 macrophages and vascular smooth muscle cells (VSMCs) without inducing cytotoxicity, and both cGRP-EVs and uncarboxylated GRP-EVs reduced pro-inflammatory cytokine release while exerting dual anti-inflammatory and anti-mineralizing effects. This study establishes the first bioengineered platform capable of generating functional

* Corresponding author at: Centro de Ciências do Mar do Algarve (CCMAR/CIMAR LA), Campus de Gambelas, Universidade do Algarve, 8005-139, Faro, Portugal.
*E-mail address:* caviegas@ualg.pt (C. Viegas).

https://doi.org/10.1016/j.bioadv.2026.214833
Received 12 January 2026; Received in revised form 3 March 2026; Accepted 16 March 2026
Available online 18 March 2026

γ-carboxylated GRP and its vesicular formulation, providing a dual innovation for VKDP research and therapeutic biomaterial development.

## 1. Introduction

Gla-rich protein (GRP), also known as upper zone of growth plate and cartilage matrix–associated protein (UCMA) [1,2], is a circulating vitamin K–dependent protein (VKDP) that plays a central role in the regulation of tissue mineralization and inflammation [3–8]. GRP functions as a potent inhibitor of ectopic calcification, acting at both local and systemic levels [3–6], and exerts anti-inflammatory effects in diverse cell types, including monocytes, macrophages, chondrocytes, synoviocytes, and vascular smooth muscle cells (VSMCs) [4,6–8]. Elevated GRP levels are generally associated with protective or homeostatic effects, whereas decreased expression or deficiency has been linked to disease progression [3–10]. These activities are particularly relevant in chronic inflammatory and calcification-related disorders such as cardiovascular disease, osteoarthritis, rheumatoid arthritis, and chronic kidney disease (CKD). Importantly, clinical data from CKD cohorts support the role of GRP as a biomarker of vascular and valvular calcification and renal dysfunction [11–13]. Given its dual anti-calcifying and anti-inflammatory properties, GRP holds significant therapeutic promise. However, its limited solubility at physiological pH [1,8] presents a major barrier to biomedical formulation and delivery, underscoring the need for optimized production and stabilization strategies.

Human GRP is synthesized as a prepropeptide and secreted as a mature protein of approximately 9.5 kDa, containing 15 potential γ-carboxylation sites within its 74–amino acid sequence, which confer strong calcium-binding capacity [1]. Like other members of the VKDP family, GRP requires post-translational γ-carboxylation of specific glutamate residues into γ-carboxyglutamate (Gla) residues for full bioactivity [3,4]. This modification depends on the coordinated action of γ-glutamyl carboxylase enzyme (GGCX) and vitamin K epoxide reductase complex subunit 1 (VKORC1, further designated as VKOR), which regenerate the reduced form of vitamin K necessary for GGCX activity [14,15]. Importantly, while the γ-carboxylated form of GRP has been shown essential for GRP mineralization-inhibitory activity [3–6], undercarboxylated GRP also displays anti-inflammatory properties [6–8], indicating that these two functional roles may be partially independent. Proper processing and secretion of GRP also require proteolytic removal of its propeptide region by the convertase Furin [1,2]. While mammalian expression systems provide the necessary enzymatic machinery, they often yield low quantities of protein and incomplete γ-carboxylation, limiting production scalability [16–18]. Co-expression of GGCX, VKOR, and Furin can enhance γ-carboxylation efficiency, but such approaches remain technically challenging and costly for large-scale applications [19–22].

The baculovirus expression vector system (BEVS) in insect cells has emerged as powerful tools for recombinant protein production, combining high yield, scalability, and safety [23–26]. Insect cells such as *Spodoptera frugiperda* (Sf9) and *Trichoplusia ni* (Hi5) can perform many mammalian-like post-translational modifications, but their capacity to support vitamin K–dependent γ-carboxylation remains uncertain [27–29]. While some studies report detectable carboxylase activity in *Drosophila* S2 cells [30,31], others indicate that functional expression of mammalian VKDPs in insect systems requires co-expression of human GGCX and VKOR, along with vitamin K supplementation [32–34]. These discrepancies underscore the need to systematically evaluate and optimize BEVS-based strategies for the functional production of complex VKDPs such as GRP.

In parallel, extracellular vesicles (EVs) have gained increasing attention as natural nanocarriers for the intercellular transport of proteins, lipids, and nucleic acids [35,36]. Their intrinsic biocompatibility, stability, and capacity to deliver bioactive molecules position them as promising tools for therapeutic delivery [36–38]. Interestingly, GRP has been identified in EVs derived from various human cell types as well as in circulating EVs, suggesting a physiological role for vesicle-mediated transport and extracellular function [3,4,7,39]. Building on this concept, we hypothesized that the baculovirus/insect cell expression system could be adapted not only to produce γ-carboxylated GRP (cGRP) but also to promote its incorporation into secreted extracellular vesicles, generating bioengineered GRP-enriched EVs (cGRP-EVs). This strategy aimed to create a cell-derived biomaterial platform capable of coupling post-translational maturation with biogenic encapsulation of functional proteins. By integrating the expression of vitamin K–dependent GRP with its natural EV packaging, this system offers a new route for producing bioactive nanoscale carriers with potential applications in the modulation of inflammation and pathological calcification, which are processes central to many chronic inflammatory diseases.

## 2. Material and methods

### 2.1. Baculovirus expression

General procedures for the manipulation of insect cells, generation and amplification of recombinant baculoviruses and protein production were performed as previously detailed [23]. To produce GRP, the cDNA encoding GRP-Flag was inserted under the control of the PH promoter using the BamHI and *Xba*I restriction sites of the pAC8_MF transfer vector [40], leading to the pAC8_MF-GFP plasmid.

To co-express GRP, Furin, GGCX and VKOR, the cDNA encoding GRP-Flag was first inserted under the control of the PH promoter using the BamHI and XbaI restriction sites while the cDNA encoding Furin-His was cloned under the control of the p10 promoter using the *Nhe*I and *Xho*I sites of the pAC8_MF transfer vector, leading to the pMF-GRP-Furin plasmid. The VKOR-His cDNA was then inserted under the control of the PH promoter and the cDNA GGCX-His under the dependence of the promoter of the pSPL transfer vector [41] leading to pSPL-GGCX-VKOR plasmid. The pMF-GRP-Furin and the pSPL-GGCX-VKOR plasmid were then fused using Cre-mediated recombination yielding the pMF-GRP-Furin-GGCX-VKOR plasmid (Fig. S1).

To co-express GRP and Furin, the cDNAs encoding the GRP-Flag-mCherry fusion protein and Furin connected by a 75 base pair linker containing the T2A peptide were cloned into the pTriex/pOPIN plasmid resulting in the pGRP-mCh/Furin transfer vector. Deletion of G 1159 introduces a frameshift resulting in the pGRP-mCh*/Furin transfer vector. It encodes the GRP-Flag-mCherry fusion protein in which the 4 carboxy-terminal residues of the mCherry protein are replaced by an 11 residue peptide whose sequence is unrelated to that of the T2A peptide. The coding sequence of Furin including the start codon is not affected. As above, to co-expresss GGCX and VKOR, the cDNAs encoding GGCX fused to a C-terminal E6 epitope and VKOR to at C-terminal HA tag were connected by a T2A-containing coding sequence and cloned into the pTriex/pOPIN plasmid resulting in the pGGCX/VKOR transfer vector. The coding sequences of the three plasmids are provided as supplementary data (Fig. S1).

Recombinant baculoviruses were generated by co-transfection of the transfer vectors with the AcMNPV BAC10:KO1629 Δv-cath/chiA bacmids [40]. The High Five™ insect cells (Hi5, BTI-TN-5B1-4) grown in suspension in Express Five™ SFM (Gibco cat.no. 10486025) media supplemented with 16 mM GltutaMAX (Gibco cat.no. 35050061) were infected with the corresponding virus. Where indicated, cell culture media were supplemented with vitamin K1 (Sigma-Aldrich, St. Louis, MO, USA; cat.no. 47773) at a final concentration of 10 μM. Typically,

cells were cultured in 1 L Erlenmeyer flasks containing 100 mL of medium and infected at a density of $1 \times 10^6$ cells/mL with 4 mL of P1 virus stock (titer ~$5 \times 10^7$ pfu/mL), corresponding to a multiplicity of infection (MOI) of 2.

Cells were harvested after 4 days of incubation at 27 °C by centrifugation at 1000 ×*g* for 10 min and washed with phosphate-buffered saline (PBS).

### 2.2. Analysis of protein expression and GRP purification from the cell culture media

To validate recombinant expression of Furin, GGCX and VKOR, cell pellets were resuspended in RIPA buffer (20 mM Tris-HCl pH 7.5, 120 mM KCl, 1% NP-40, 0.1% SDS, 1 mM EDTA, 0.5% sodium deoxycholate, and protease inhibitor cocktail [5× PIC]) and incubated on ice for 30 min with occasional pipetting. Lysates were clarified by centrifugation at 14,000 ×*g* for 20 min. Protein concentration was determined using a Bradford assay. A total of 20 µg of protein was analysed by Western blot, as described below, using the following antibodies: anti-Furin, anti-HA, and anti-E6.

To validate expression and/or purify the GRP-Flag and GRP-Flag-mCherry fusion protein, conditioned media were incubated with anti-FLAG® M2 affinity beads (Sigma-Aldrich, cat.no. A2220) for 5 h at 4 °C with gentle agitation. We typically use 40 µL of resin for 10 mL of medium. After extensive wash with PBS, bound proteins were eluted using 0.1 M glycine-HCl (pH 2.5) or 0.2 mg/mL competitor peptide (DYKDDDDK) in PBS. Eluates were analysed by Western blot, as described below, using anti-FLAG® M2, CTerm-GRP and M3B antibodies.

### 2.3. Extracellular vesicles (EVs) isolation

EVs were isolated from Hi5 cells culture media by differential ultracentrifugation at 100.000 ×*g* in the case of GRP-flag overexpression systems, or at 30.000 ×*g* followed by 100.000 ×*g* in GRP-mCherry overexpression systems, according to previously described procedures [4,39]. In either case, EVs were isolated from conditioned media after GRP anti-FLAG® M2 affinity capture, starting with an initial centrifugation at 2500 rpm for 30 min at 4 °C, with the recovered supernatants either directly centrifuged at 100.000 ×*g* for 2 h or, centrifuged at 30.000 ×*g* for 30 min (30 K EVs) followed by centrifugation at 100.000 ×*g* for 2 h (100 K EVs). Centrifugations at 30.000 and 100.000 ×*g* were performed at 4 °C in a Beckman Otima XPN100 ultracentrifuge (Beckman Coulter, Brea, CA, USA) using the T70 fixed angel rotor. All EV pellets at 30 K and 100 K were washed with PBS and re-centrifuged in the respective conditions in a Beckman Otima Max XP micro-ultracentrifuge using the TLA-55 fixed angel rotor. All EV pellets were resuspended in PBS, aliquoted and immediately stored at −80 °C until further use. EVs were independently isolated three times ($n = 3$), each isolation starting with 25 mL of cell culture media.

### 2.4. Total protein extraction and quantification

Total protein extracts from isolated EVs were obtained with RIPA buffer as described [3,4,39]. Isolated EVs total protein quantity was also directly quantified in intact EVs resuspended in PBS. VSMCs protein extracts were obtained after demineralization with 1 M HCl using 1 M NaOH with 5% (*w/v*) SDS for neutralization and extraction. In all cases, total protein quantification was determined by the MicroBCA protein assay kit (Thermo Fisher Scientific, Pierce, Rockford, IL, USA) and used either to infer EVs quantity or to normalize GRP, calcium and pro-inflammatory cytokines data.

### 2.5. GRP quantification by ELISA

GRP was quantified in EVs RIPA total protein extracts, using a specific and validated ELISA assay for total GRP (GenoGla Diagnostics) [4]. GRP levels were normalized to respective total protein content and are presented as GRP/total protein ratios.

### 2.6. Electrophoresis and Western blot

Aliquots of 20 µg of Hi5 cells protein extracts, 15–20 µL of immunoaffinity captured GRP from the cell media (described above), 5–10 µg of EVs total protein extracts, and 15 µg of VSMCs total protein extracts were size-separated on a NuPAGE 4–12% (w/v) gradient polyacrylamide precast gels containing 0.1% (w/v) SDS (Invitrogen, Thermo Fisher Scientific, Waltham, MA, USA) and either stained with G-250 Coomassie brilliant blue or transferred onto a nitrocellulose membrane (Bio-Rad Laboratories, Hercules, CA, USA) as previously described [3,4]. Target protein detections were performed through overnight incubation with primary anti-Furin (Santa Cruz Biotechnology, SC-133142; 1 µg/mL), anti-HA (IGBMC, 12CA5; 1 µg/mL), anti-E6 (IGBMC, 1E6F4; 1 µg/mL), anti-FLAG® M2 (Sigma-Aldrich, cat.no. F3165; 1 µg/mL), CTerm-GRP (GenoGla Diagnostics, Faro, Portugal; 5 µg/mL), anti-CD9 (Santa Cruz Biotechnology, SC-9148; 1:200), anti-Gla residues M3B (BioMedica Diagnostics Windsor, NS, Canada; cat.no. 3570; 5 µg/mL), anti-RUNX2 (Santa Cruz Biotechnology, SC-101145; 1:200) and anti-mCherry (Invitrogen; PA5-34974; 1:6000) antibodies. Immunodetection was achieved using species-specific secondary horseradish peroxidase-conjugated antibodies and Western Lightning Plus-ECL (PerkinElmer, Waltham, MA, USA). Image acquisition was obtained using an IQ LAS 4000 mini biomolecular imager (GE Healthcare, Chicago, IL, USA).

### 2.7. RNA extraction and qPCR

Aliquots of isolated EVs were incubated with RNase A (Thermo Fisher Scientific; 0.5 mg/mL) for 20 min at 37 °C to degrade unprotected RNA. RNA was extracted using Direct-zol RNA Miniprep kit (Zymo Research, Irvine, CA, USA), according to the manufacturer's instructions. The RNA concentration was determined by spectrophotometric analysis at 260 nm using a Nanodrop spectrophometer (Thermo Fisher Scientific). 250 nanograms of total RNA were treated with RQ1 RNase-free DNase (Promega, Madison, WI, USA) and reverse-transcribed as described [4]. Real-time PCR was performed in a CFX Connect™ Real-Time PCR detection system (Bio-Rad) with SsoFast EvaGreen Supermix (Bio-Rad), and GRP specific primers (GRP_1F: 5′-GTCCCCCAAGTCCCGAGATGAGG-3′ and GRP_1R: 5′-CCTCCACGAAGTTCTCAAATTCATTCC-3′), and previously described conditions [4,8]. Fluorescence was measured at the end of each extension cycle in the FAM-490 channel and melting profiles of each reaction were performed to check for unspecific product amplification.

### 2.8. Nanoparticle tracking analysis

The concentration and size distribution of 30 K and 100 K EVs particles was performed by Nanoparticle Tracking Analysis (NTA) using NanoSight NS300™ (Malvern Instruments, UK) equipment. The samples were diluted with 0.22 µm filtered DPBS (Gibco, Thermo Fisher Scientific) to be in the instrument's linear range of $1 \times 10^8$–$1 \times 10^9$ particles/mL. Each sample was analysed in triplicate with independent dilutions. Capture settings (shutter and gain) were adjusted manually for each analysis and all steps were carried out at room temperature. For each measurement, three 30-second videos were recorded and analysed with the Nanoparticle Tracking Analysis (NTA) 2.3 Analytical software considering a size range for EVs between 50 and 200 nm. To facilitate comparison of size distribution profiles between 30 K and 100 K EV samples, NTA measurements were normalized against total particle concentration and expressed as relative concentration.

### 2.9. Transmission electron microscopy (TEM) and immunogold labelling

Isolated EVs were adsorbed onto formvar-carbon coated grids and stained with 1% aqueous uranyl acetate. The grids were air dried, observed and photographed in a JEOL 1200EX transmission electron microscope. Immunogold labelling for GRP in EVs was performed using a previously described method [4]. Briefly, blocked grids were incubated with the CTerm-GRP antibody (5 μg/mL) for 1 h at RT, followed by incubation with the secondary anti-rabbit 10-nm gold antibody (Sigma-Aldrich; 1:15) for 1 h at RT.

### 2.10. Proteomic analysis of gel bands

Proteomics analysis to characterize secreted recombinant GRP-Flag (GRP-F) was carried out at LSMBO, France (Laboratory 1) and of GRP-Flag-mCherry (GRP-mCh) at VIB, Belgium (Laboratory 2). The following description integrates both experimental procedures, with laboratory-specific parameters indicated where needed.

In-gel digestion was performed using a standard tryptic digestion workflow. Gel bands were excised and subjected to sequential washing steps to remove contaminants. In Laboratory 1, gel pieces were washed twice with 25 mM ammonium hydrogen carbonate ($NH_4HCO_3$) and acetonitrile (ACN), whereas in Laboratory 2, gel bands were washed sequentially with water, 50% ACN, and 100% ACN, followed by complete dehydration in a vacuum concentrator.

Cysteine residues were reduced and alkylated in Laboratory 1 using dithiothreitol (10 mM, 57 °C) and iodoacetamide (55 mM), respectively. In Laboratory 2, no reduction and alkylation steps were performed. Following dehydration, proteins were digested in-gel using modified porcine trypsin (Promega, Madison, WI, USA). In Laboratory 1, digestion was performed using trypsin at 12.5 ng/μL in 25 mM $NH_4HCO_3$ overnight at room temperature, whereas in Laboratory 2, gel bands were rehydrated with trypsin at a final concentration of 0.005 μg/μL in 50 mM ammonium bicarbonate (pH 8) and incubated overnight at 37 °C.

Tryptic peptides were extracted using acidified organic solvent. In Laboratory 1, peptides were extracted with 60% ACN in 0.1% formic acid, whereas in Laboratory 2, peptide-containing supernatants were acidified to pH 2–3 using formic acid to terminate digestion. Peptide solutions were dried under vacuum prior to LC–MS/MS analysis.

Peptide separation was performed by nanoLC using reversed-phase chromatography with laboratory-specific solvent systems and gradients. In Laboratory 1, analyses were carried out on a nanoACQUITY UPLC system (Waters, Milford, MA, USA) equipped with an ACQUITY UPLC® CSH130 C18 analytical column (250 mm × 75 μm, 1.7 μm particle size) and a Symmetry C18 trapping column (20 mm × 180 μm, 5 μm particle size). The mobile phases consisted of solvent A (0.1% formic acid in water) and solvent B (0.1% formic acid in ACN). Samples were loaded for 3 min at 5 μL/min using 99% solvent A, followed by peptide elution at a flow rate of 300 nL/min using an 8–35% linear gradient of solvent B over 9 min. In Laboratory 2, samples were analysed on an Ultimate 3000 RSLC nanoLC system (Thermo Fisher Scientific, Germany) using an in-house packed C18 trapping column (100 μm I.D. × 20 mm, 5 μm beads, Reprosil-HD) coupled to a 200 cm μPAC™ C18 analytical column (PharmaFluidics, Belgium) maintained at 50 °C. The mobile phases consisted of solvent A′ (0.1% formic acid in water) and solvent B′ (0.1% formic acid in water/ ACN, 20/80 [v/v]). Peptides were eluted using a linear gradient from 98% solvent A′ to 55% solvent B′ at 65 min, followed by an increase to 70% solvent B′ at 70 min and a re-equilibration with solvent A′ at 80 min. The first 15 min the flow rate was set to 500 nl/min after which it was kept constant at 300 nL/min.

Mass spectrometric analysis was performed in positive ion mode using data-dependent acquisition. In Laboratory 1, the nanoLC system was coupled to a TripleTOF 5600 mass spectrometer (SCIEX, Framingham, MA, USA) operated in information-dependent acquisition (IDA) mode using a Top10 method. MS survey scans were acquired over the *m/z* 400–1250 range, followed by MS/MS scans over the m/z 150–1800 range, with dynamic exclusion set to 4 s. External calibration was performed using digested bovine serum albumin peptides. In Laboratory 2, the nanoLC system was coupled to a Q Exactive HF BioPharma mass spectrometer (Thermo Fisher Scientific). Full-scan MS spectra (375–1500 m/z) were acquired at a resolution of 60,000 in the Orbitrap analyzer after accumulation to a target value of 3E6. The 12 most intense ions above a threshold value of 1.3E4 were isolated with a width of 1.5 m/z for fragmentation at a normalized collision energy of 30% after filling the trap at a target value of 100,000 for maximum 80 ms. MS/MS spectra (200–2000 m/z) were acquired at a resolution of 15,000 in the Orbitrap analyzer. The polydimethylcyclosiloxane background ion at 445.120028 Da was used for internal calibration (lock mass) and QCloud has been used to control instrument longitudinal performance during the project [42,43].

Raw mass spectrometry data were processed using laboratory-specific software pipelines. In Laboratory 1, raw data collected were converted to. mgf peak list format using MSDataConverter. and searched with MASCOT software (version 2.4.1). The database used was extracted from UniProtKB (human taxonomy Uniprot release of 14th March 2016). Semi-trypsin was selected as cleavage enzyme and a maximum of one missed cleavage was allowed. For MS/MS parameters, a parent mass tolerance of 10 ppm and a fragment mass tolerance of 0.05 Da were used allowing a maximum of one trypsin missed cleavage. Carbamidomethylation of cysteine residues and oxidation of methionine residues were specified as variable modifications. Protein identifications were validated with at least two peptides with Mascot ion score above 25. In Laboratory 2, raw data were analysed using MaxQuant software (version 2.0.3.0) with predominantly default search settings, including a false discovery rate (FDR) of 1% applied at the peptide-spectrum match (PSM) and protein levels. Spectra were searched against the GRP-mCherry construct sequence, as well as the *Spodoptera frugiperda* UniProt/Swiss-Prot database (August 2022 release, 26,917 protein sequences). Variable modifications were set to carboxylation of glutamic acid residues, oxidation of methionines, propionamide on cysteines and acetylation of protein N-termini. Matching between runs was enabled with a matching time window of 0.7 min and an alignment time window of 20 min.

### 2.11. Proteomic analysis of EVs

EV samples were re-suspended in 4 mL lysis buffer (1 mg/mL amphipol A8–35 (Anatrace) in 50 mM ammonium bicarbonate pH 8.0) and further processed as described [44]. Briefly, lysates were sonicated with a PIXUL Multisample sonicator (Active Motif) for 10 min with default settings (Pulse 50 cycles, PRF 1 kHz, Burst Rate 20 Hz) and centrifuged for 10 min at 20,000 ×*g* at 4 °C to remove insoluble material. The protein concentration in the supernatants was measured with the Pierce Microplate BCA Protein Assay Kit (Reducing Agent Compatible, Thermo Fisher Scientific), following the manufacturer's protocol. The proteins (50 μg per sample) were reduced by addition of 15 mM DTT and incubation for 30 min at 55 °C, and then alkylated by addition of 30 mM iodoacetamide and incubation for 15 min at room temperature in the dark. Proteins were then digested with 0.5 μg lysyl endopeptidase (Wako) for 4 h at 37 °C, followed by overnight digestion with 0.5 μg trypsin (Promega) at 37 °C. Samples were acidified with TFA to a f.c. of 1% (pH < 3.0), incubated for 15 min on ice and centrifuged for 10 min at 20,000 ×*g* and RT to pellet the precipitated Amphipol A8–35. Supernatants were purified on Omix C18 tips (Agilent) and the purified peptides were dried completely by vacuum drying and stored at −20°C. Peptides were re-dissolved in 20 μL loading solvent A (0.1% trifluoroacetic acid in water/acetonitrile (ACN) (98:2, v/v)) of which 5 μL was injected for LC-MS/MS analysis on an Ultimate 3000 Pro Flow nanoLC system in-line connected to a Q Exactive HF mass spectrometer (Thermo). Trapping was performed at 20 μL/min for 2 min in loading solvent A on a 5 mm trapping column (Thermo scientific, 300 μm internal diameter (I.D.), 5 μm beads). The peptides were separated on a

250 mm Aurora Ultimate, 1.7 μm C18, 75 μm inner diameter (Ionopticks) kept at a constant temperature of 45 °C in a butterfly oven (Phoenix S&T). Peptides were eluted by a non-linear gradient starting at 0.5% MS solvent B reaching 26% MS solvent B (0.1% FA in acetonitrile) in 75 min, 44% MS solvent B (0.1% FA in acetonitrile) in 95 min, 56% MS solvent B in 100 min followed by a 5-minute wash at 56% MS solvent B and re-equilibration with MS solvent A (0.1% FA in water) at a constant flowrate of 250 nl/min.

The mass spectrometer was operated in data-dependent mode using the same method described in Section 2.10 for Laboratory 2.

Analysis of the mass spectrometry data was performed in MaxQuant (version 2.3.1.0) with mainly default search settings including a false discovery rate set at 1% on PSM and protein level. Spectra were searched twice against different protein sequence databases. In a first analysis, the database included the human reference proteome, the *Trichoplusia ni* reference proteome and the *Autographa californica nuclear polyhedrosis virus* (AcMNPV) proteome (version of June 2024, 20,594, 20,889 and 155 entries, respectively). In the second (main) analysis, only human and *T. ni* protein sequences were used, together with the GRP-mCherry construct sequence. The mass tolerance for precursor and fragment ions was set to 4.5 and 20 ppm, respectively, during the main search. Enzyme specificity was set as C-terminal to arginine and lysine, also allowing cleavage at proline bonds with a maximum of two missed cleavages. Cysteine carbamidomethylation was set as a fixed modification, variable modifications were set to oxidation of methionine residues and acetylation of protein N-termini. Matching between runs was enabled with a matching time window of 0.7 min and an alignment time window of 20 min. Only proteins with at least one unique or razor peptide were retained. Proteins were quantified by the MaxLFQ algorithm integrated in the MaxQuant software. A minimum ratio count of two unique or razor peptides was required for quantification. A total of 211,442 and 213,596 peptide-to-spectrum matches (PSMs) was detected, resulting in 30,239 and 25,717 identified peptides, corresponding to 3033 and 2843 identified proteins, respectively for the first and the second analysis (Tables S1.1-2). Further data analysis of the shotgun results was performed with an in-house R script, using the proteinGroups output table from MaxQuant. Reverse database hits were removed, iBAQ intensities were log2 transformed and normalized with median subtraction and replicate samples were grouped. Proteins with one valid iBAQ quantification value were kept and missing values were imputed from a normal distribution centered around the detection limit (package DEP), leading to a list of 2835 quantified proteins in the experiment, used for further data analysis. Differential abundance analysis between EVs 100 K and EVs 30 K sample groups was performed with the package limma, with a false discovery rate (FDR) $<0.05$ and a fold change of $>4$- or $<0.25$-fold ($|\log2FC| = 2$) used as cut-off values for statistical significance. Results are presented in Table S1.3. Z-scored iBAQ intensities from significantly regulated proteins and belonging to the top 100 Vesiclepedia protein list (version of May 2024) were plotted in a heatmap after non-supervised hierarchical clustering. Identification of human orthologs for *T. ni* was carried out based on the BLASTp algorithm, using the reciprocal best hit approach [45].

### 2.12. Cell culture

THP-1 cell line was cultured according to ATCC instructions in RPMI Growth Medium (RPMI 1640 with L-Glutamine (Gibco), 10% heat-inactivated Fetal Bovine Serum (FBS, Biowest), 1% (v/v) Pen-Strep (P/S, Gibco). THP-1 macrophage differentiation (THP-1 Mac) was achieved by culturing cells in 25 ng/mL of phorbol 12-myristate 13-acetate (PMA) (Sigma-Aldrich) in complete RPMI for 48 h.

Human aortic VSMCs (VSMC) derived from tissue explants as described previously [46] were kindly provided by Prof. Dr. Leon Schurgers, Department of Biochemistry, CARIM, Maastricht University, The Netherlands, and used between passages 7 and 14. VSMCs were maintained in M199 medium (Life Technologies) supplemented with 10% FBS and 1% (v/v) of P/S.

All cell cultures were maintained at 37 °C in a humidified atmosphere containing 5% $CO_2$, and for all experiments, cells were cultured with EVs-depleted FBS through centrifugation at 100.000 $\times g$ for 24 h in a Beckman Otima XPN100 ultracentrifuge using the T70 fixed angel rotor.

### 2.13. Measurements of intracellular and extracellular kinetic profiles of mCherry fluorescence

THP-1 Mac were seeded into black 96-well plates (Thermo Scientific Nunc) and cultured with complete RPMI media without phenol red, with or without supplementation with EVs containing 10 ng/mL of GRP as quantified by ELISA, over a 72 h time course. At each time point, conditioned culture media were collected, and cells were washed 2 times with PBS and maintained in HBSS (Gibco) for immediately fluorescence measurements. Fluorescence of 100 uL of each conditioned culture media in black 96-well plates were also recorded. mCherry fluorescence measurements of cells and conditioned media were performed using an excitation wavelength/bandwidth of 590/20 nm and emission wavelength/bandwidth of 645/40 nm [47] in a Synergy2 microplate reader (BioTek, Winooski, VT, USA). After each measurement, Hanks' balanced salt solution (HBSS) was removed from the cells and the collected conditioned media added again to the respective conditions.

### 2.14. Flow cytometry analysis

To assess cellular binding of GRP-mCherry–loaded EVs, 30 K and 100 K EV populations containing 10 ng/mL GRP-mCherry were incubated with $5 \times 10^5$ THP-1 Mac or confluent VSMCs in 24-well plates containing 500 μL of culture medium for 24 h. After incubation, cells were trypsinized, pelleted, and blocked with 0.5% BSA in PBS for 30 min at room temperature, followed by fixation in 2% PFA in PBS overnight at 4 °C. A permeabilization step was then performed using 0.1% Triton X-100 in PBS for 10 min. Cells were incubated with the anti-mCherry antibody (1:400) for 1 h at 4 °C, washed with 0.1% Triton X-100 in PBS, and then stained with an Alexa Fluor® 647–conjugated donkey anti-rabbit IgG secondary antibody (0.5 μg/mL, BioLegend, cat. no. 406414) for 30 min at 4 °C. After final washes, cells were resuspended in PBS and analysed on a CytoFLEX flow cytometer (Beckman Coulter), equipped with the 488 nm, 638 nm and 405 nm lasers. Data collection and analysis were performed using CytExpert software. Control conditions were included to account for background signal and ensure accurate gating. These consisted of cells without EVs treatment in three different conditions: i) unstained cells; ii) cells incubated with the secondary antibody; and iii) cells incubated with primary and secondary antibodies. For each experimental condition 10,000 gated events were recorded. Three independent experiments using EVs from three independent isolations, each with duplicates per condition, were performed in THP-1 Mac, and two independent experiments, each with a single replicate per condition were conducted in VSMCs.

### 2.15. Fluorescence microscopy

VSMCs were plated at low density on 24-well plates with coverslips coated with 0.01% gelatin and allowed to adhere for 24 h. Culture medium was replaced with fresh medium containing 30 K and 100 K EVs (10 ng/mL GRP-mCherry). After 24 h of exposure, cells were washed with PBS, fixed with 4% paraformaldehyde (PFA) at 4 °C for 30 min, and washed again with PBS. Nuclear staining was performed with DAPI (Sigma-Aldrich; 1:1000) for 5 min at RT, protected from light. Coverslips were then washed and mounted with glycerol on microscope slides and sealed.

Fluorescence and phase contrast images were acquired using an inverted microscope (Zeiss AxioVert.A1.FL) equipped with Axiocam202 camera and appropriate filter sets for DAPI (Ex 390/40 | BS 420 | EM BP

450/40) and mCherry (Ex BP 560/40 | BS 585 | EM BP 630/75). Images were acquired with A-plan 100×/1.25 Ph3 objective (pixel size 93 nm) with 20 ms exposure times for DAPI images and 150 ms for mCherry channel in a 12-bit grayscale format. Fluorescence intensity of mCherry-positive EV aggregates were detected by TrackMate [48] in FIJI (ImageJ), using an estimated object diameter of 0.5 μm and quality threshold of 35, allowing for subpixel localization. Each detected aggregate is quantified as mean intensity per detected spot (Mean Intensity, A.U.), and it is represented in logarithmic scale to account for the log-normal distribution of fluorescence values. Data were analysed using GraphPad Prism and include the total number of spots detected across all analysed images from two independent experiments, with the number of analysed images per condition indicated.

### 2.16. Cell viability

Cells were seeded in 96-well plates at $2.5 \times 10^5$ cells/well and cultured in 200 μL of the corresponding cell culture media and supplemented with different concentrations of 30 K and 100 K EVs as quantified by NTA (ranging from $1 \times 10^8$ to $7.5 \times 10^9$ particles/mL) for 48 h. Cell media were collected for pro-inflammatory cytokine quantification by ELISA as described below. Cell viability was determined using the CellTiter 96 cell proliferation assay (Promega, Madison, WI, USA), following manufacturer's instructions. Cells without any treatment were used as control cells with 100% cell viability. Three independent experiments using EVs from three independent isolations, each with duplicates per condition, were performed.

### 2.17. Inflammatory assays in THP-1 differentiated macrophages (THP1-Mac)

The inflammatory potential of isolated EVs was evaluated in $2.5 \times 10^5$ THP1-Mac cells plated in 96-well plates with 200 μL media, by treatments with different concentrations of GRP-mCherry-EVs, considering GRP (0.1–1 ng/mL) as the quantification normalizing factor for each population, for 24 h. 30 K and 100 K EVs from Crl-mCherry not containing GRP were normalized for particle concentration and used as the maximum number of particles required for EVs loaded with GRP. Inflammation was stimulated with lipopolysaccharide (LPS O111:B4; Sigma-Aldrich, L4391) (100 ng/mL) for additional 24 h. Cell media were recovered and used for tumor necrosis factor-alpha (TNFα) quantification by ELISA as described below. Three independent experiments using EVs from three independent isolations, each with triplicates per condition, were performed.

### 2.18. VSMCs calcification assays

VSMCs were either cultured in control or mineralizing (MM) conditions by media supplementation with 2.5 mmol/L NaH2PO4 during 13 days with media changed every 3 days, and then supplementation with 3.6 mmol/L CaCl2 for 24 h, as previously described [4,39]. For the evaluation of the effect of GRP-F-EVs from the GRP-F/Furin/GGCX/VKOR baculoviruses system, 5 μg of total EVs protein were used in three independent experiments. In the case of cGRP-mCh- and ucGRP-mCh-EVs, EVs containing GRP at concentrations from 0.1 to 1 ng/mL, and Crl-mCherry EVs at the equivalent maximum particles/mL were used. In both cases EVs were added to MM cells at the beginning of the experiments and at every medium change. At least three independent experiments using GRP-mCh-EVs from three independent isolations, each with triplicates per condition, were performed. At the end of the experiments, cell media were collected for interleukin-6 (IL-6) quantification, and cells were washed 2 times with PBS for calcium and protein quantification. Calcium quantification was performed using a commercially available kit (Randox Laboratories Ltd., Crumlin, UK) based on the O-cresolphatein complexone according to manufacturer's recommendations, after extracellular matrix demineralization with 1 M HCl for 48 h at 4 °C.

### 2.19. Quantification of pro-inflammatory mediators by ELISA

Collected cell culture media were centrifuged at 16.000 ×*g* for 20 min at 4 °C to remove cellular debris and used for quantification of TNFα and IL-6 by ELISA (R&D Systems, Minneapolis, MN, USA), following the manufacture's protocols.

### 2.20. Statistical analysis

Statistical analysis was performed using PRISM software (GraphPad). Data are presented as mean ± standard deviation (SD). Student's *t*-test was used for comparison between two groups. For more than two groups significance was determined using ordinary one-way ANOVA with comparison between groups by Dunnett test. Statistical significance was defined as $p \leq 0.05$ (*), $p \leq 0.01$ (**) and $p \leq 0.001$ (***) and $p \leq 0.0001$ (****).

## 3. Results

### 3.1. Development of a baculovirus expression vector system (BEVS) to enable post-translational maturation of human Gla rich protein (GRP)

To establish an insect cell–based platform capable of producing functional γ-carboxylated Gla-rich protein (cGRP), we engineered a baculovirus co-expression system that mimics the mammalian γ-carboxylation and propeptide-cleavage machinery. Specifically, recombinant baculoviruses were constructed to enable the co-expression of human GRP together with γ-glutamyl carboxylase (GGCX), vitamin K 2,3-epoxide reductase (VKOR), and the proprotein convertase Furin.

As detailed in the Materials and Method section, we relied on cre-mediated recombineering to fuse an acceptor vector containing the expression cassettes for GRP fused to a C-terminal Flag tag and Furin (pMF GRP-F/Furin) with a donor plasmid for the co-expression of GGCX and VKOR (pSPL GGCX/VKOR) and generated the corresponding virus by homologous recombination (Fig. 1A, B). The GRP cDNA was fused to a Flag-affinity tag (GRP-F) which was added at the C-terminus of the protein to avoid interference with the signal peptide and propeptide located at the N-terminal region.

To evaluate the capacity of insect cells to produce and gamma-carboxylate recombinant GRP, Hi5 cells were then infected by a virus encoding GRP-F, Furin, GGCX and VKOR (virus GRP-F/Furin/GGCX/VKOR) with or without vitamin K supplementation. Cells were also infected with a virus containing only the expression cassette for GRP (virus GRP-F) to evaluate endogenous post translational processing capacity. Culture media were collected after 96 h incubation and secreted GRP-Flag proteins (GRP-F) were isolated from the conditioned media by immunoprecipitation (IP) with the anti-FLAG® M2 antibody.

Western blot analysis using the CTerm-GRP antibody detecting total GRP [4,49], showed the presence of two positive bands with an apparent molecular mass of approximately 15 and 20 kDa in cells infected with GRP-F virus, marked as 1 and 2 on the SDS-PAGE gel, and a single band of approximately 15 kDa when the four proteins are co-expressed, marked as 3 in the SDS-PAGE gel (Fig. 1C, D). No major differences were observed with or without vitamin K treatments. However, a single positive band of around 15 kDa, corresponding to band 3 in the SDS-PAGE gel, was detected with the gamma-carboxylation specific M3B antibody [49], only when GRP-F is co-expressed with Furin, GGCX and VKOR, in the presence of vitamin K (Fig. 1C, D). MS/MS analysis of SDS-PAGE gel slices marked as 1, 2 and 3 identified human GRP protein in all bands with a sequence coverage between 49 and 87%, but with different proteolytic processing. In addition to peptides which map the sequence of the mature protein identified in all bands, GRP sequence in band 1 included the signal peptide and propeptide regions, only propeptide region in band 2, and only the mature form in band 3 (Figs. 1E and S2).

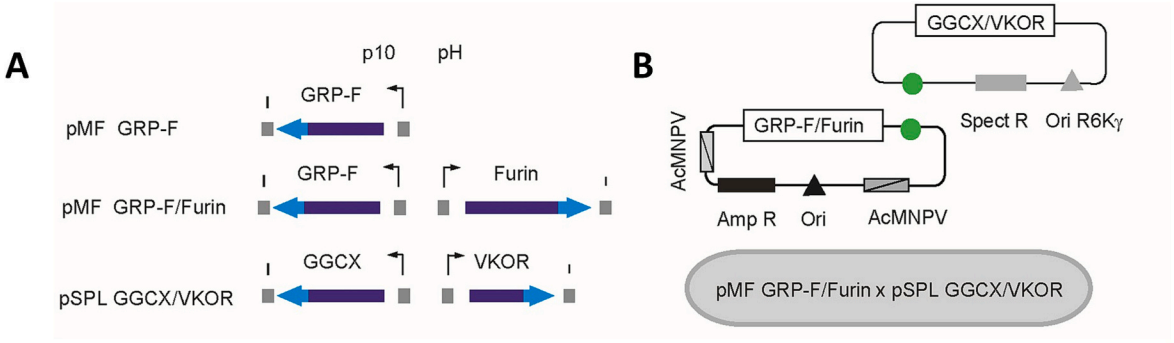


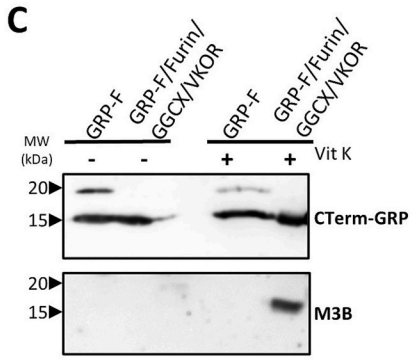


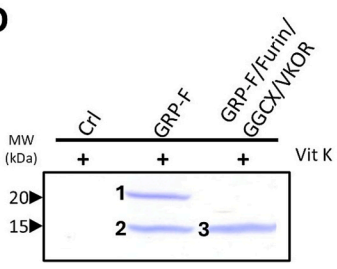



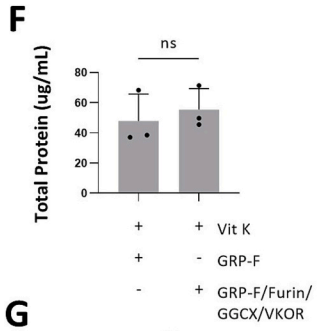


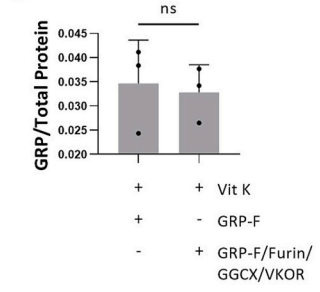


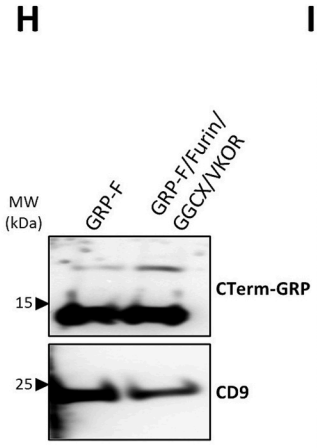


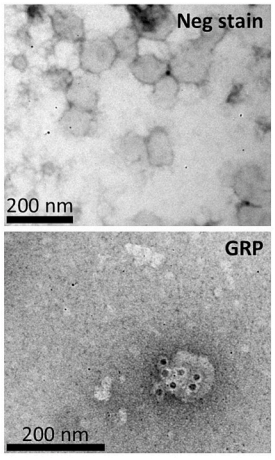


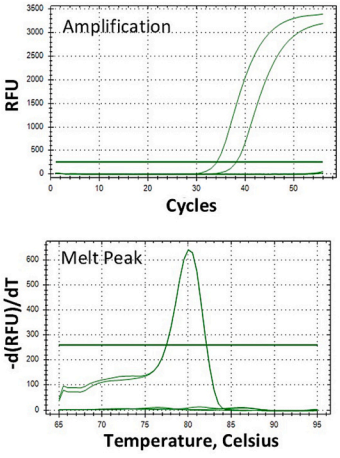


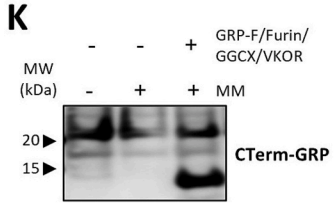


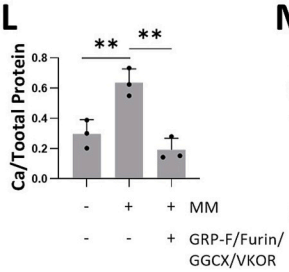


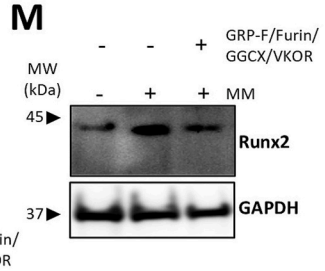


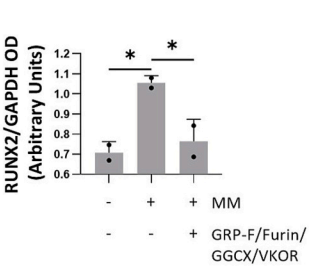


*(caption on next page)*

**Fig. 1.** Bioengineered baculovirus–insect cell system for the production of γ-carboxylated GRP and GRP-associated EVs. (A–B) Schematic representation of the recombinant transfer vectors encoding GRP-Flag (GRP-F), GRP-F/Furin and GGCX/VKOR expression cassettes, and the Cre-mediated recombineering strategy used for generation of the recombinant baculovirus. Green circles, loxP sites. (C) Western blot of immunoprecipitated GRP-F from conditioned media of Hi5 cells infected with GRP-F or GRP-F/Furin/GGCX/VKOR baculoviruses, ± vitamin K, probed with CTerm-GRP (total GRP) and M3B (anti-Gla residues) antibodies. (D) SDS-PAGE of vitamin K treated samples described in C panel showing three main bands (1–3). (E) Schematic representation of GRP forms identified by MS/MS analysis of bands marked in panel D, indicating signal peptide (SP), propeptide (PP), and mature peptide (MP) regions. (F) Total protein quantification of EVs isolated at 100.000 ×*g* from GRP-F and GRP-F/Furin/GGCX/VKOR cultures ($n = 3$). (G) GRP levels quantified by ELISA normalized to total protein in isolated EVs (n = 3). (H) Western blot of EV fractions to detect GRP and the EV marker CD9. (I) Transmission electron microscopy (TEM) of negatively stained EVs (upper) and GRP immunogold labelling (lower). (J) RT-qPCR amplification and melt-curve analysis of human GRP mRNA detected in EVs. (K) Detection of GRP with the CTerm-GRP antibody in lysates of VSMCs cultured under mineralizing conditions (MM) for 14 days in the presence of GRP-EVs from GRP-F/Furin/GGCX/VKOR baculoviruses system (n = 3). (L) Calcium quantification normalized to total protein in VSMCs under mineralizing conditions (n = 3). (M–N) RUNX2 expression in mineralizing VSMCs assessed by Western blot and densitometric analysis ($n = 2$). Data are expressed as mean ± SD. *ns*, non-significant.

These findings demonstrate that this BEVS, when supplemented with vitamin K1, is able to produce and secrete post-translationally modified human GRP with γ-carboxylation and propeptide cleavage, supporting its suitability for functional protein production.

### 3.2. BEVS-derived extracellular vesicles carry GRP cargo and exhibit proof-of-concept functional activity in mineralizing VSMCs

Because extracellular vesicles (EVs) are natural carriers for many secreted proteins, and GRP has previously been identified in EVs released by several mammalian cell types and detected in circulation [3,4,7,39], we next investigated whether GRP expressed by BEVS was associated with secreted EVs. For that, EVs were isolated from the culture media of vitamin K–supplemented Hi5 cells infected with either GRP-F or GRP-F/Furin/GGCX/VKOR recombinant viruses, and subsequently analysed for the presence of GRP. Quantification of total protein in EVs isolated at 100,000 ×g suggested a similar yield of EVs from both systems (Fig. 1F). GRP levels normalized to total protein content were also comparable between conditions (Fig. 1G). In addition, Western blot using the C-Term GRP antibody revealed a predominant band of approximately 15 kDa in EVs from both GRP-F and GRP-F/Furin/GGCX/VKOR conditions, and the presence of the EV marker CD9 (Fig. 1H). TEM of negatively stained EVs revealed small, intact vesicles with limited size heterogeneity (Fig. 1I). Positive detection of GRP by immunogold labelling reinforces the presence of GRP protein associated to these EVs (Fig. 1I).

Because EVs are known to carry nucleic acids including mRNA, the presence of human GRP mRNA in RNase A treated EVs was assessed by RT-qPCR. Positive amplification with a specific melting profile indicated the presence of GRP mRNA in EVs isolated from Hi5 cells infected with both GRP-F and GRP-F/Furin/GGCX/VKOR (Fig. 1J). Together, these results indicate that BEVS-derived EVs represent a dual source of GRP cargo, carrying both GRP protein and GRP mRNA, thereby suggesting that this system may serve as a potential platform for EV-based delivery.

To further assess whether BEVS-derived GRP-containing EVs exert biological activity in recipient cells, EVs isolated from Hi5 cells infected with GRP-F/Furin/GGCX/VKOR were applied to human primary vascular smooth muscle cells (VSMCs) cultured under mineralizing conditions. A GRP-positive band of approximately 15 kDa was only detected in VSMC lysates following EV treatment, indicating association of EV-derived GRP with recipient cells (Fig. 1K). Functionally, GRP-containing EVs reduced calcium deposition as compared to mineralizing medium alone (Fig. 1L). In parallel, expression of the osteogenic transcription factor RUNX2 was decreased in EV-treated VSMCs relative to mineralizing controls, as shown by Western blot and densitometric analysis (Fig. 1M, N). These results provide initial functional evidence that BEVS-derived GRP-EVs retain biological activity in recipient VSMCs and can attenuate osteogenic programming under calcifying conditions.

### 3.3. GGCX/VKOR co-expression and vitamin K supplementation enable GRP γ-carboxylation, while Furin mediates propeptide cleavage

Having established the BEVS platform for production of gamma-carboxylated GRP in insect cells and its incorporation into secreted EVs, GRP was fused to a C-terminal mCherry (mCh) tag to facilitate GRP tracking. To co-express the GRP-mCh with GGCX, VKOR and Furin, we constructed two bicistronic baculoviruses in which two cDNAs were linked with a T2A self-cleavage peptide sequence to be used to co-infect Hi5 cells (Fig. 2A). We first verified that the first virus expresses GGCX-E6 and VKOR-HA (GGCX/VKOR) and that the second produces the target GRP-mCh and the Furin coding gene (GRP-mCh/Furin) (Fig. 2B). Of note, one virus construct GRP-mCh*/Furin contained a frameshift after the GRP-mCh coding sequence, resulting in significant reduction but not abolishment of Furin expression (Fig. 2B), since the Furin gene retained an almost consensus Kozak sequence (Fig. S1).

Next, Hi5 cells were infected with Ctrl-mCh, GRP-mCh*/Furin, GRP-mCh*/Furin/GGCX/VKOR, and GRP-mCh/Furin/GGCX/VKOR. Infection with GRP-mCh*/Furin without vitamin K supplementation was performed as a negative control to gamma-carboxylation. GRP produced in the different systems was characterized by SDS-PAGE (Fig. 2C), Western blot (Fig. 2D), and MS/MS (Fig. 2E) following immunoprecipitation of Flag-tagged proteins from cell culture media. SDS-PAGE analysis revealed two major protein bands between 37 and 50 kDa, consistent with the theoretical molecular weight of the GRP-mCh fusion protein (approximately 40–47 kDa, depending on GRP post translational processing). Similar migration profiles were observed for GRP-mCh*/Furin with and without vitamin K supplementation, as well as for the GRP-mCh*/Furin + GGCX/VKOR condition (Fig. 2C, bands 1–6), with all bands testing positive for both GRP and mCherry (Fig. 2D). In the GRP-mCh/Furin + GGCX/VKOR condition, a single band within the same molecular weight range was detected (Fig. 2C, band 7), also positive for GRP and mCherry (Fig. 2D). γ-carboxylation with the M3B antibody was only detected in bands 5 and 6 from GRP-mCh*/Furin + GGCX/VKOR and band 7 from GRP-mCh/Furin+ GGCX/VKOR systems (Fig. 2D).

MS/MS analysis of SDS-PAGE 1–7 gel slices marked in Fig. 2C identified GRP-mCherry peptides located within the mature protein in all bands (Fig. 2E and Fig. S3). Peptides on the signal peptide region were identified in bands 1 and 3, while bands 1–6 include peptides spanning the propeptide region. Band 7 contained peptides exclusively from the mature protein (Figs. 2E and S3). Overall, these results showed that vitamin K supplementation with co-expression of GGCX and VKOR are required for GRP gamma-carboxylation and suggested that Furin expression plays a critical role in propeptide cleavage of the secreted protein. The incomplete processing observed with GRP-mCh*/Furin, where propeptide-derived peptides were still detected by MS/MS, contrasts with the complete maturation seen with GRP-mCh/Furin, which yielded peptides exclusively within the mature GRP region.

### 3.4. Morphological and molecular characterization of EVs released from BEVS

Given the growing interest in insect-cell EVs as bioengineering tools, we next performed a comprehensive morphological and proteomic characterization of BEVS-derived vesicles. Differential ultracentrifugation at 30,000 ×*g* (30 K) followed by 100,000 ×g (100 K) was used to

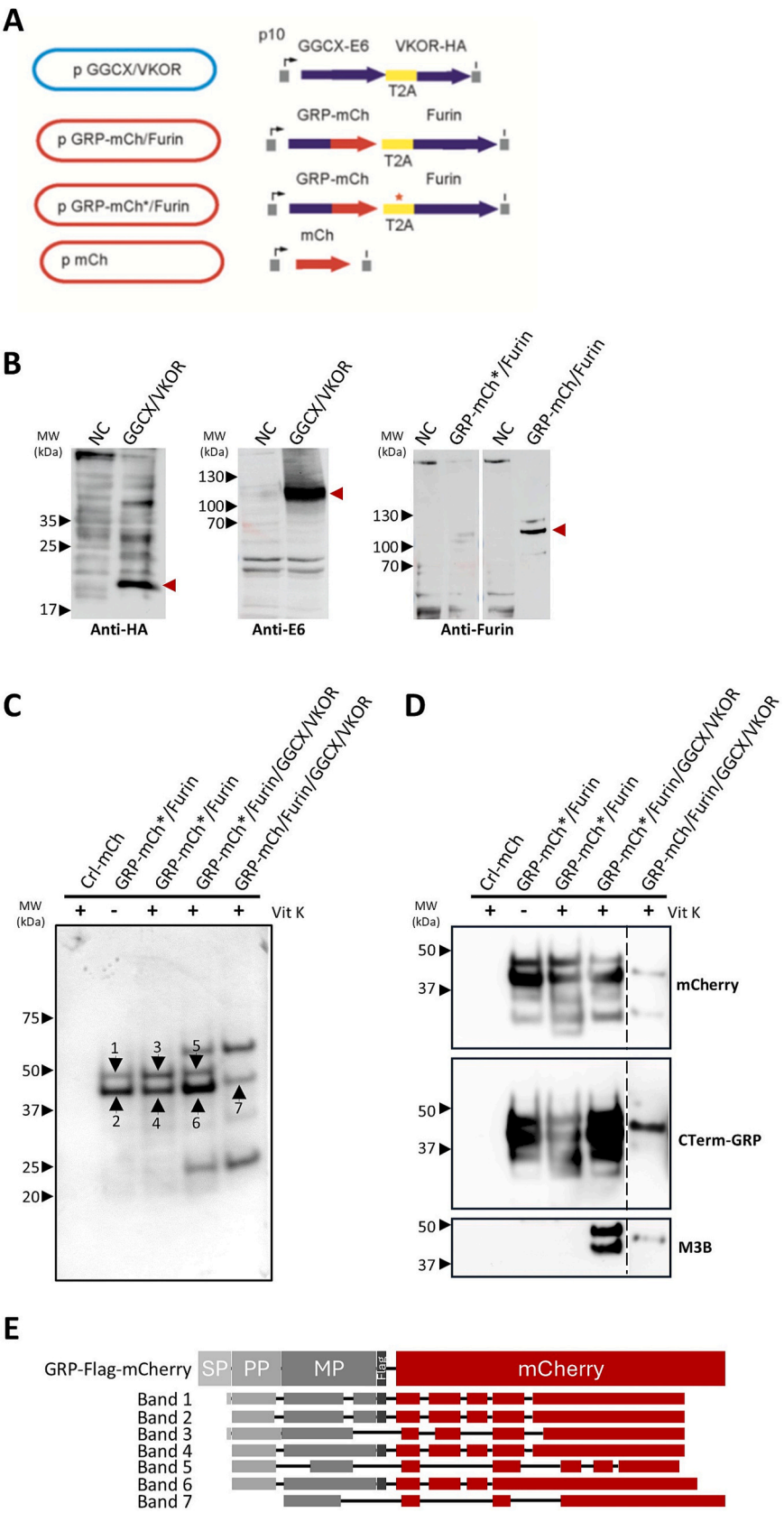


*(caption on next page)*

**Fig. 2.** Co-expression of GGCX/VKOR and Furin enables γ-carboxylation and maturation of GRP-mCherry in the BEVS platform. (A) Schematic representation of recombinant baculovirus transfer vectors encoding bicistronic expression cassettes for GGCX/VKOR and GRP-mCherry (GRP-mCh)/Furin (including GRP-mCh*/Furin with a frameshift after mCherry). (B) Western blot analysis confirming expression of VKOR-HA, GGCX-E6, GRP-mCh, and Furin in Hi5 cells infected with the respective viruses. (C) SDS-PAGE of secreted Flag-tagged GRP-mCh proteins immunoprecipitated from culture media of Hi5 cells infected with Ctrl-mCh, GRP-mCh*/Furin ± vitamin K, GRP-mCh*/Furin + GGCX/VKOR, and GRP-mCh/Furin + GGCX/VKOR viruses. (D) Western blot analysis of corresponding samples using CTerm-GRP, anti-mCherry, and M3B antibodies. (E) Schematic mapping of MS/MS-identified GRP peptides obtained from gel bands 1–7 (panel C), showing their localization to signal peptide (SP), propeptide (PP), and mature protein (MP) regions of GRP fused to mCherry.

separate larger and smaller vesicles, respectively, thereby reducing sample complexity and heterogeneity [39,50–53].

EVs quantification and size distribution by NTA showed differences between Crl-mCh EVs and EVs isolated from GRP-mCherry over-expression systems (Fig. 3A and Table S2). Crl-mCh EVs, both 30 K and 100 K, presented similar unimodal size distributions and concentrations. In contrast, EVs from GRP-mCherry-overexpressing systems displayed broader, more complex size distributions, with 100 K EVs exhibiting higher particle concentrations as compared to 30 K EVs. Notably, most particles were 50–200 nm in size, accounting for 78–92% of 30 K and 88–95% of 100 K EV populations (Table S2). TEM analysis confirmed the presence of small, intact vesicles exhibiting the typical cup-shaped morphology, mostly below 200 nm in size, with no major differences observed between 30 K and 100 K EVs across samples (Fig. 3B).

Proteome characterization of isolated EV populations was performed by shotgun proteomics, with spectra initially searched against protein databases for *Trichoplusia ni*, *Homo sapiens*, and *Autographa californica* multiple nucleopolyhedrovirus (AcMNPV). A total of 3033 proteins were identified across all samples (Table S1.1), primarily matching *T. ni* sequences, along with detectable viral proteins from AcMNPV, fewer human matches, and a small number of ambiguous entries (Fig. 3C). Because the focus of this study is the host and recombinant human protein content of EVs, subsequent analyses were concentrated on 2835 protein groups of *T. ni* and *H. sapiens* origin that had at least one valid quantification value in either experimental condition (Table S1.1, 1.2). Principal component analysis revealed clear clustering of 30 K and 100 K EV proteomes (Fig. 3D), with differential expression patterns further distinguishing these populations (Fig. 3E). To confirm the extracellular vesicle nature of the isolated populations, we examined the presence of known EV proteins from the top 100 Vesiclepedia list. We identified 52 of these proteins, including commonly known EV markers such as CD63, syntenin-1 (SDCBP), programmed cell death 6-interacting protein (PDCD6IP), flotillin-1 (FLOT1), tumor susceptibility gene 101 protein (TSG101), and ADAM10 (Table S1.3). Of these, 51 were common to both 30 K and 100 K EVs, while alpha-actinin-1 (ACTN1) was uniquely detected in 30 K EVs (Fig. 3F). Notably, expression patterns of these markers clearly distinguished the two EV populations (Fig. 3G).

These analyses establish the first detailed molecular characterization of BEVS-derived EVs, revealing distinct 30 K and 100 K populations enriched in canonical EV markers, suitable for downstream biofunctionalization.

### 3.5. GRP preferentially associates with 30 K EVs and undergoes γ-carboxylation under optimized co-expression conditions

Characterization of GRP-mCherry loaded into the different EVs populations was performed through ELISA, Western blot and proteomic analysis (Fig. 4). EVs total protein quantification showed higher protein levels in 100 K EVs relative to 30 K in all populations (Fig. 4A), in line with the EVs concentrations determined by NTA. However, GRP levels were found consistently higher in 30 K EVs suggesting preferential enrichment of GRP in these populations (Fig. 4B). Comparison of the 30 K EVs between overexpression systems demonstrates lower GRP levels in GRP-mCh/Furin/GGCX/VKOR. As expected, GRP levels in Crl-mCh EVs were below the limit of quantification. No significant differences in GRP levels were found in both populations of GRP-mCh*/Furin EVs with or without vitamin K treatments (Fig. 4B). The SDS-PAGE protein profile showed distinct protein profile patterns across the different EV populations, but within each 30 K and 100 K groups the patterns were mostly similar (Fig. 4C). This is consistent with the proteomic data indicating distinguishable proteomes for 30 K and 100 K EVs. Detection of GRP-mCherry by western blot with both anti-mCherry and the CTerm-GRP antibodies revealed a migration pattern similar to that previously obtained for GRP-mCherry secreted into the cell media. Specifically, two protein bands between 37 and 50 kDa in 30 K and 100 K EVs from GRP-mCh*/Furin/GGCX/VKOR and GRP-mCh*/Furin with or without vitamin K treatment, while a single band was detected in 30 K EVs from GRP-mCh/Furin/GGCX/VKOR cell system (Fig. 4D). Higher intensity in GRP-mCherry detection found in the 30 K EVs is consistent with the ELISA data. Absence of GRP-mCherry detection by western blot in 100 K EVs from GRP-mCh/Furin/GGCX/VKOR was most likely due to the low levels of GRP in this population. Absence of mCherry detection in Crl-mCh EVs suggests that mCherry is not loaded at significant levels into EVs in this cell system. GRP-mCherry γ-carboxylation was only detected in the cell systems overexpressing GGCX and VKOR, particularly in the 30 K EVs containing higher GRP-mCherry protein levels (Fig. 4D). MS/MS data from shotgun analysis identified GRP-mCherry as the 70th most abundant protein in the entire data set, with a coverage of 76% with 34 GRP identified peptides (Table S3). Analysis of the specific identified GRP peptides revealed the presence of one peptide corresponding to the propeptide region in all EVs populations, suggesting that at least part of GRP is not processed by Furin before its loading into EVs (Table S3). Analysis of peptides intensity of GRP-mCherry fusion protein reinforce its preferential loading into 30 K EVs (Fig. 4E). An apparent detection of low-level GRP-mCherry in Crl-mCh EVs is due to the identification of mCherry peptides in this condition. However, in the case of sample 30 K Crl-mCh, there were two detected peptides mapping to GRP protein sequence, which we attribute to a possible contamination of the analytical column coming from the previously analysed sample 30 K GRP-mCh*/Furin without vitamin K, the second one with the highest levels of GRP-mCherry/total protein (Fig. 4B). The absence of mCherry detection by Western blot and positive MS identification in Crl-mCh EVs, indicates low mCherry loading into EVs when overexpressed alone. In addition, GGCX, VKOR and Furin were also identified in EV populations isolated from systems overexpressing these enzymes, with all proteins preferentially associated with 30 K EVs (Fig. 4E). Higher Furin peptide intensity in GRP-mCh/Furin/GGCX/VKOR confirmed increased protein production relative to GRP-mCh*/Furin/GGCX/VKOR.

Overall, following the proof-of-concept and characterization of GRP overexpression using the BEVS platform, we demonstrated that cGRP is produced in vitamin K–treated cells co-expressing GGCX and VKOR. Importantly, cGRP is released into the culture media both as a “free” protein and selectively loaded into specific EV populations. Furthermore, all heterologous proteins expressed were efficiently targeted to EVs, with a preferential enrichment in the 30 K EV population. Altogether, these data demonstrate that BEVS can produce γ-carboxylated GRP efficiently targeted to 30 K EVs, positioning these vesicles as promising carriers for functional VKDP delivery.

### 3.6. GRP-loaded EVs decreased pro-inflammatory reactions in THP-1-derived macrophage

To assess the inflammatory functional relevance of BEVS-derived GRP-EVs, we evaluated their anti-inflammatory potential in LPS-stimulated THP-1 macrophages, where GRP has been shown to function as an anti-inflammatory agent independently of its γ-carboxylation

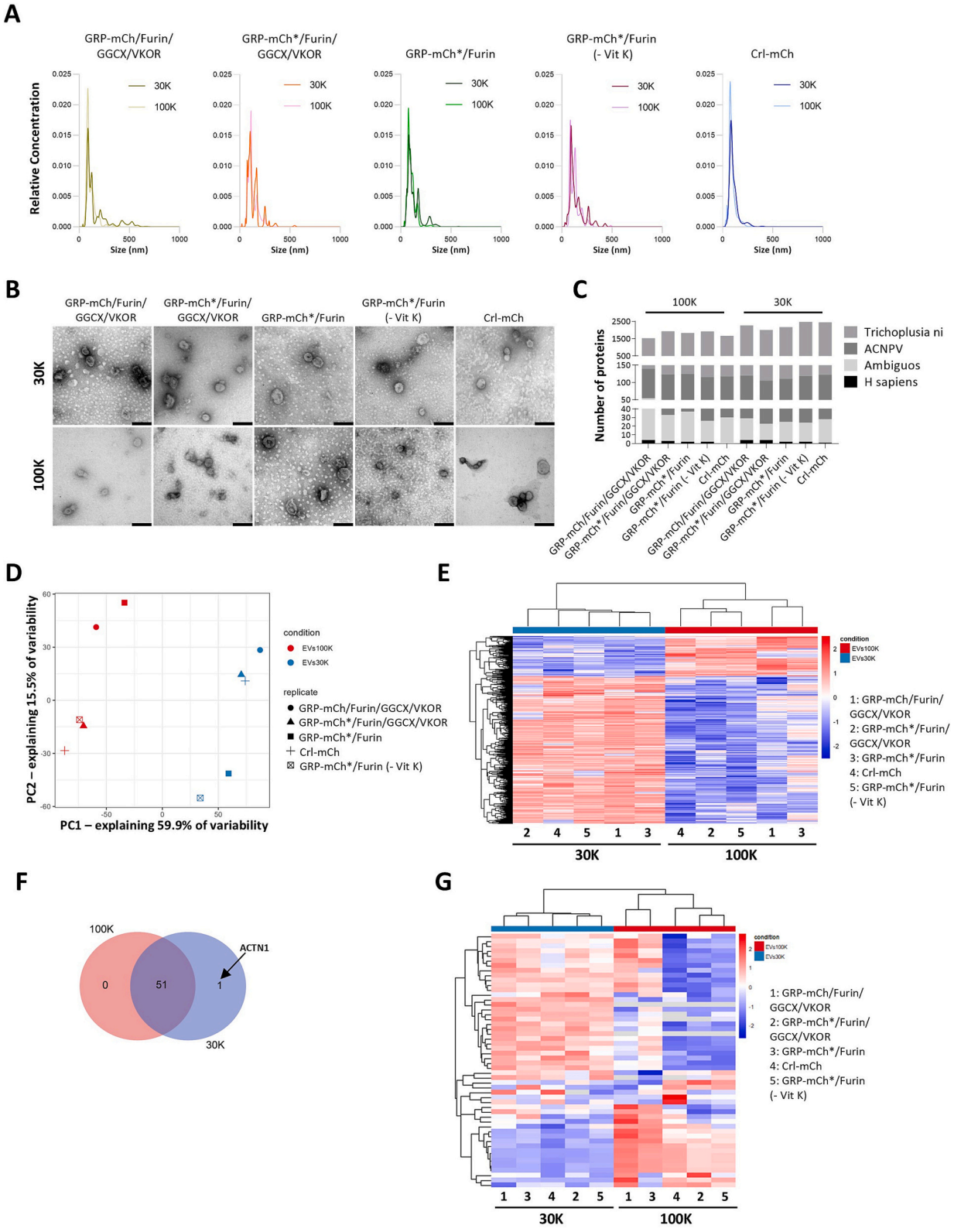


**Fig. 3.** Morphological and molecular characterization of engineered EVs released from BEVS. (A) Nanoparticle tracking analysis (NTA) of EVs isolated by differential ultracentrifugation at 30,000 ×*g* (30 K) and 100,000 ×*g* (100 K) from control (Ctrl-mCh) and GRP-mCherry overexpression systems. Relative concentrations and particle size distributions are shown for each condition. (B) Transmission electron microscopy (TEM) of negatively stained 30 K and 100 K EVs. Scale bars, 200 nm. (C) Summary of protein identifications across EV samples based on database searches against *Trichoplusia ni*, *Homo sapiens*, and *Autographa californica* multiple nucleopolyhedrovirus (AcMNPV). (D) Principal component analysis (PCA) of quantified EV proteomes, based on log2 IBAQ protein intensities. (E) Hierarchical clustering heatmap of z-scored iBAQ intensities for differentially expressed proteins (adj.*p*-value<0.05, |log2 fold-change|>2), distinguishing 30 K and 100 K EVs. (F) Venn diagram showing overlap of top 100 Vesiclepedia EV proteins identified in 30 K and 100 K EVs; ACTN1, alpha-actinin-1. (G) Hierarchical clustering heatmap of z-scored iBAQ intensities for canonical EV markers detected in BEVS-derived vesicles, illustrating distinct expression profiles between 30 K and 100 K populations.

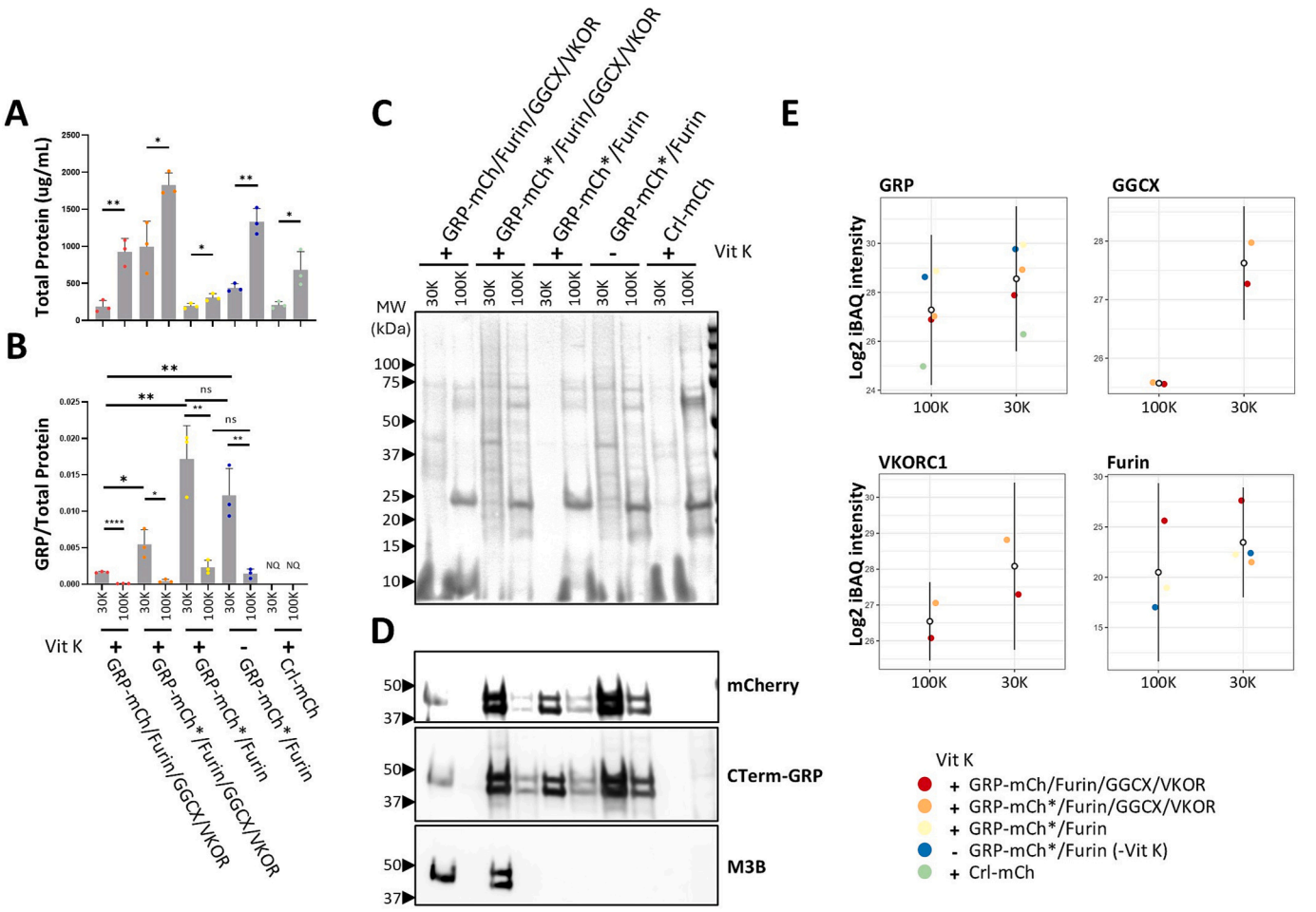


**Fig. 4.** GRP preferentially associates with 30 K EVs and undergoes γ-carboxylation under optimized co-expression conditions. (A) Total protein content of 30 K and 100 K EVs isolated from control (Ctrl-mCh) and GRP-mCherry overexpression systems (n = 3 independent isolations). (B) Quantification of GRP levels by ELISA normalized to total protein in 30 K and 100 K EVs (n = 3). Data are expressed as mean ± SD. Statistical significance: $^{*}p < 0.05$, $^{**}p < 0.01$, $^{****}p < 0.0001$. NQ, not quantifiable GRP. (C) Representative SDS-PAGE profiles of 30 K and 100 K EV proteins. (D) Western blot analysis of GRP-mCherry using anti-mCherry, CTerm-GRP, and M3B antibodies. (E) Normalized protein intensities for GRP-mCherry, GGCX, VKOR, and Furin across 30 K and 100 K EV samples.

status [6–8]. Here, we tested the anti-inflammatory potential of EVs loaded with cGRP-mCherry (cGRP-mCh) (isolated from GRP-mCh*/Furin/GGCX/VKOR with vitamin K treatment) and ucGRP-mCherry (ucGRP-mCh) (isolated from GRP-mCh*/Furin without vitamin K treatment) in LPS-stimulated THP-1-derived macrophages (THP-1 Mac). EVs from Crl-mCh were used as negative controls for GRP.

First, GRP delivery to THP-1 Mac was assessed by monitoring mCherry fluorescence in both cells (Fig. 5A) and culture media (Fig. 5B) over 72 h following treatment with EVs normalized to contain equivalent GRP amounts (based on ELISA quantification). Increased cellular mCherry signal was detectable as early as 30 min post-treatment for all EV populations, with similar kinetic profiles between EVs isolated using the same centrifugal forces (30 K versus 100 K), and peak intensities at 4 h for 100 K EVs and 24 h for 30 K EVs. Decreased fluorescence intensity was observed from 24 h onward, reaching levels similar to non-treated control cells by 72 h. As expected, a progressive decrease in fluorescence intensity was also observed in the cell media, particularly up to 24 h (Fig. 5B). In addition, flow cytometry of THP-1 Mac treated for 24 h with the different EV populations was performed to detect mCherry using an anti-mCherry antibody and Alexa Fluor® 647-conjugated secondary antibody. Representative dot plots show a clear increase in APC-positive events in all EV-treated samples compared to the double-stained negative control, confirming the presence of GRP-mCherry signal after EV exposure (Fig. 5C). Quantification of APC-positive events, normalized to the control, revealed comparable GRP-mCherry detection across 30 K and 100 K cGRP- and ucGRP-EV populations, indicating similar delivery efficiency among the different vesicle fractions (Fig. 5D).

An important aspect when considering functional effects in any cell system treated with heterologous EVs, such as those from insect origin, is potential toxicity. In this context, EV toxicity in THP-1 Mac was evaluated across a wide range of particle concentrations after 48 h of treatment. Cell viability was not significantly altered by any of the EV populations at the concentrations tested, compared to untreated THP-1 Mac (Fig. 5E). Although a tendency toward reduced viability was observed at higher EV concentrations, particularly for 100 K EVs, the lowest cell viability recorded was 79% (±4). However, analysis of TNF-α levels in the cell media revealed a marked increase in TNF-α release in THP-1 Mac exposed to the highest concentration ($7.5 \times 10^9$ particles/mL) of 100 K EVs (Fig. 5F).

To specifically test the anti-inflammatory effects of GRP-EVs, THP-1 Mac were pre-treated for 24 h with c/uc-GRP-mCh EVs at different GRP concentrations, followed by LPS stimulation for an additional 24 h. Since the main aim was to investigate the functional role of GRP, EVs were normalized to the same GRP content across all populations, regardless of particle concentration, and considering only concentrations that did not induce pro-inflammatory responses. TNF-α levels in the culture media were used as an indicator of the inflammatory status. The results showed that all EV populations containing GRP-mCh reduced TNF-α levels compared to LPS-treated cells, while EVs from Crl-mCh had no effect (Fig. 5G). Notably, the anti-inflammatory effects

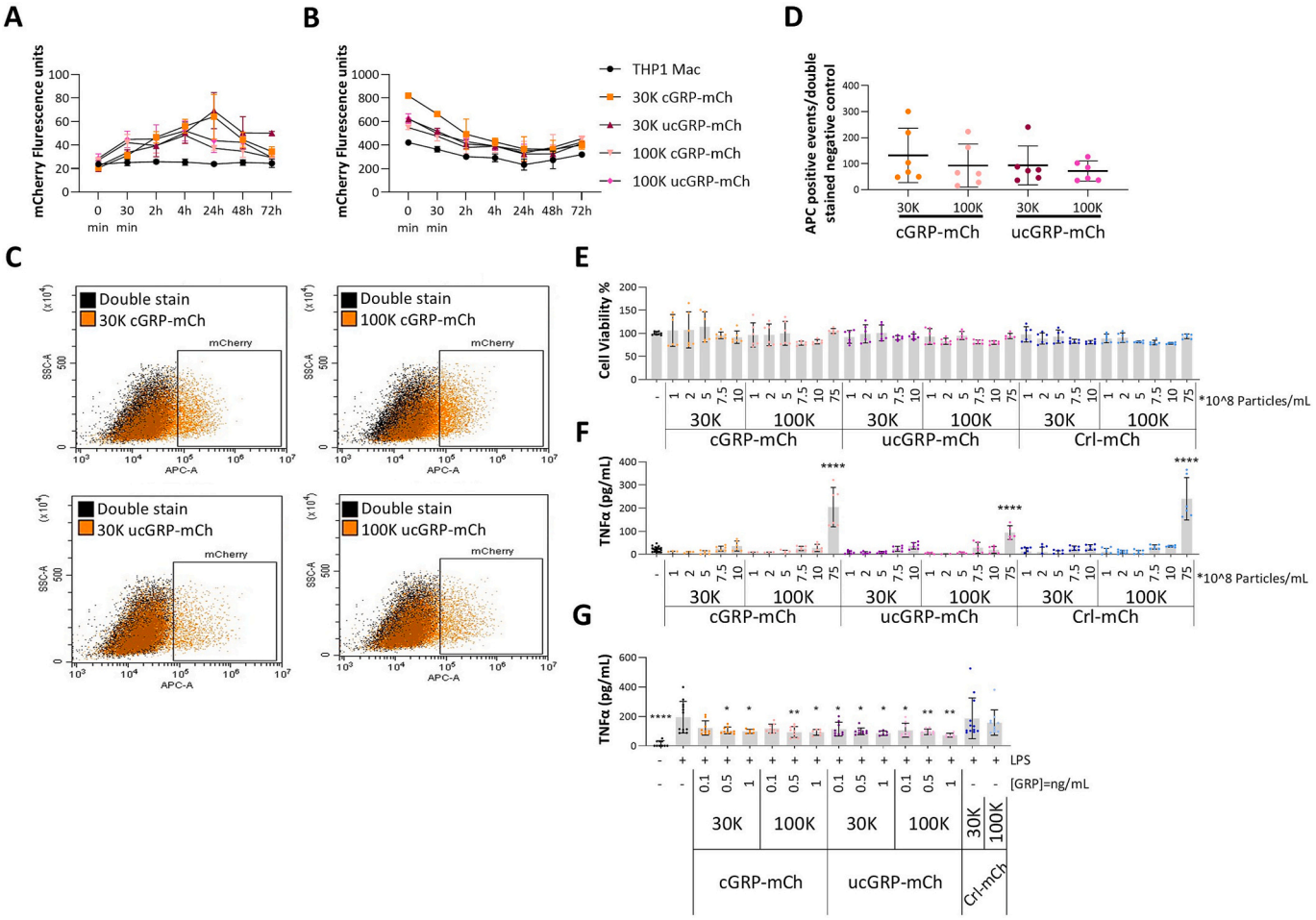


**Fig. 5.** GRP-loaded EVs attenuate pro-inflammatory responses in THP-1-derived macrophages (THP-1 Mac). (A–B) Time-course of mCherry fluorescence in THP-1 Mac (A) and corresponding culture media (B) following treatment with EVs loaded with γ-carboxylated (cGRP-mCh) or undercarboxylated (ucGRP-mCh) GRP (n = 3). (C) Representative flow cytometry dot plots showing APC–mCherry double-staining of THP-1 Mac after 24 h exposure to 30 K and 100 K cGRP- and ucGRP-EVs. (D) Quantification of APC-positive cells normalized to untreated controls (n = 3, each with duplicates). (E) Cell viability and (F) TNF-α levels of THP-1 Mac after 48 h treatment with increasing EV concentrations (n = 3, each with duplicates). (G) TNF-α levels in THP-1 Mac pre-treated with GRP-loaded (cGRP-mCh and ucGRP-mCh) and control (Crl-mCh) EVs for 24 h and stimulated with LPS for additional 24 h (n = 3, each with triplicates). Data are expressed as mean ± SD. Statistical significance: *$p < 0.05$, **$p < 0.01$, ****$p < 0.0001$ vs. control or LPS treatment.

were observed with both cGRP- and ucGRP-loaded EVs, suggesting that this activity may be less strictly dependent on γ-carboxylation. The strongest and most dose-dependent suppression of TNF-α was achieved with 100 K ucGRP-mCh EVs at GRP concentrations of 0.5 and 1 ng/mL (Fig. 5G). Similar effects were also observed using cGRP-mCh EVs from the GRP-mCh/Furin/GGCX/VKOR system, tested at 0.5 ng/mL GRP (Fig. S4).

These results demonstrate that BEVS-derived EVs carrying either cGRP or ucGRP can effectively modulate macrophage inflammation, underscoring their potential as anti-inflammatory nanotherapeutics.

### *3.7. Differential effects of γ-carboxylated and uncarboxylated GRP-loaded EVs on calcification and inflammation in human VSMCs*

Having established that BEVS-derived cGRP-containing EVs are biologically active in recipient VSMCs (Section 3.2), we next investigated whether the γ-carboxylation status of GRP influences the functional impact of GRP-EV. A key role of GRP has been attributed to its mineralization-inhibitory function, particularly within the cardiovascular system [3–5]. However, the relative contribution of carboxylated (cGRP) versus uncarboxylated (ucGRP) forms to these effects remains incompletely defined.

To address this, EVs loaded with either cGRP-mCherry (cGRP-mCh) or ucGRP-mCherry (ucGRP-mCh) were applied to human primary VSMCs cultured under pro-calcifying conditions (Fig. 6), for the evaluation of both calcium content and pro-inflammatory markers, as classical outputs in vascular-associated mineral deposition and associated inflammation.

The association of cGRP-mCh and ucGRP-mCh EVs with VSMCs was assessed through direct detection of mCherry fluorescence following 24 h of exposure, using equivalent GRP amounts across all EV populations. Fluorescence microscopy revealed distinct red puncta in cells exposed to both 30 K and 100 K EVs, whereas untreated controls showed no detectable signal (Fig. 6A). Quantification of fluorescence intensity confirmed a significant increase in mean mCherry signal in all EV-treated conditions relative to controls (Fig. 6B). These results were corroborated by flow cytometry, which showed a clear fluorescence signal in the mCherry detecting APC channel for EV-treated VSMCs compared to untreated controls (Fig. 6C), further supporting EV association with the cells.

To evaluate potential cytotoxicity, VSMCs were exposed for 48 h to increasing concentrations of the different EV populations (Fig. 6D). cGRP-mCh EVs did not significantly affect VSMC viability at any concentration tested. In contrast, ucGRP-mCh EVs induced a modest reduction in viability at higher doses, with the lowest viability (78 ± 7%) observed at the highest concentration of 30 K EVs. Notably, Crl-

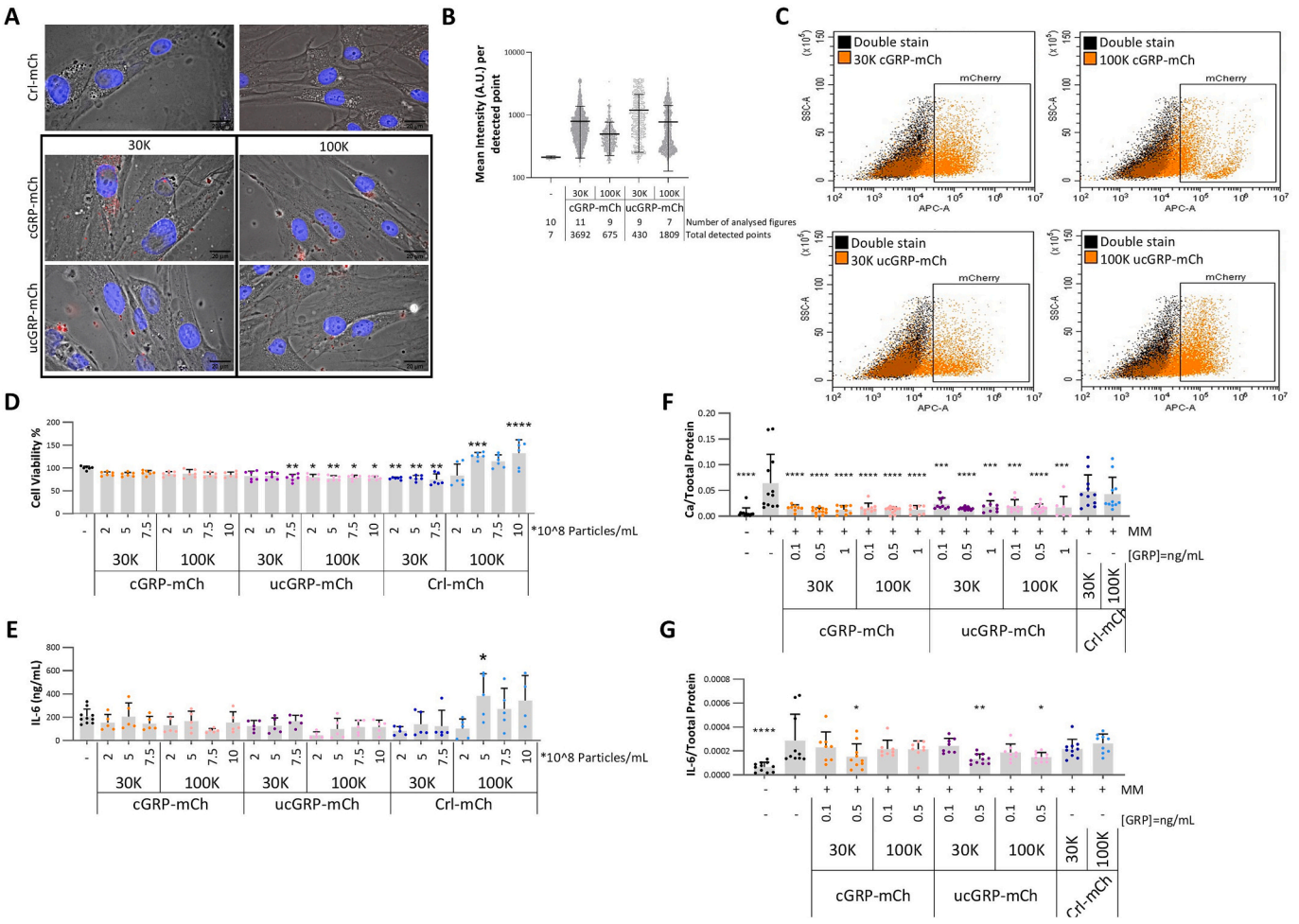


**Fig. 6.** GRP-loaded EVs associate with VSMCs and attenuate calcification and inflammation. (A–B) Fluorescence microscopy and quantification showing cellular association of mCherry-labeled cGRP-mCh and ucGRP-mCh EVs with VSMCs after 24 h (n = 2). (C) Flow cytometry detection of mCherry fluorescence confirming EV association with VSMCs (n = 2). (D) Viability of VSMCs after 48 h exposure to increasing concentrations of the indicated EV populations (n = 3, each with duplicates). (E) IL-6 release from VSMCs after 24 h treatment with GRP-mCh or control EVs (n = 3, each with duplicates). (F) Calcium deposition normalized to total protein in VSMCs cultured under mineralizing conditions (MM) for 14 days in the presence of GRP-mCh or control EVs (n = 3, each with triplicates). (G) IL-6 levels in mineralizing VSMCs treated with GRP-mCh or control EVs (n = 3, each with triplicates). Data are expressed as mean ± SD. Statistical significance: $*p < 0.05$, $**p < 0.01$, $***p < 0.001$, $****p < 0.0001$ vs. control or MM conditions.

mCh 30 K EVs caused a more pronounced viability decrease across all concentrations, whereas Crl-mCh 100 K EVs appeared to enhance cell viability, especially at higher concentrations.

IL-6 measurements in VSMC culture media revealed no increase in this pro-inflammatory cytokine upon treatment with either cGRP-mCh or ucGRP-mCh EVs (Fig. 6E). In contrast, a modest increase in IL-6 was detected in cells treated with Crl-mCh 100 K EVs.

The calcification-inhibitory activity of cGRP-mCh and ucGRP-mCh EVs was evaluated in VSMCs induced to mineralize for 14 days, with EVs replenished at each media change. As previously described, GRP-mCh EV doses were normalized to contain equivalent GRP levels at non-toxic concentrations. Both cGRP- and ucGRP-mCh EVs significantly reduced calcium (Ca) deposition, normalized to total protein, in mineralizing VSMCs compared to untreated mineralizing controls (MM), while no reduction in Ca accumulation was observed with Crl-mCh EV treatment (Fig. 6F). While both GRP-loaded EV populations attenuated calcification, cGRP-mCh EVs consistently induced a stronger effect supporting a contributory role of γ-carboxylation in modulating mineral deposition. ucGRP-mCh EVs achieved comparable inhibition only at the 0.5 ng/mL concentration for both 30 K and 100 K. In addition, cGRP-mCh EVs from the GRP-mCh/Furin/GGCX/VKOR system were also tested at 0.5 ng/mL GRP and showed similar calcification-inhibitory effects (Fig. S5).

Given the close interplay between vascular calcification and inflammation, and the proposed role of GRP as a crosstalk mediator in these processes, we next assessed the anti-inflammatory potential of GRP-loaded EVs in mineralizing VSMCs. A reduction in IL-6 accumulation was observed at the 0.5 ng/mL GRP concentration in cells treated with 30 K cGRP-mCh EVs, and in both 30 K and 100 K ucGRP-mCh EVs, compared to untreated mineralizing controls (MM). Among these, the most pronounced IL-6 decrease was achieved with the 30 K ucGRP-mCh EVs (Fig. 6G).

Collectively, these findings reveal that GRP-loaded EVs exert dual anti-calcific and anti-inflammatory effects in vascular cells, highlighting their promise as a next-generation bioengineered nanomaterial for cardiovascular protection.

## 4. Discussion

In this work, we report the development of a novel baculovirus/insect cell–based bioengineering strategy to overexpress the vitamin K–dependent protein GRP, resulting in the production of its mature and γ-carboxylated form (cGRP). Notably, cGRP is efficiently released into the extracellular medium and simultaneously incorporated into EVs

secreted by the engineered insect cells. This dual output represents a major advance, integrating the secretion of a functional VKDP with its EV packaging into a single, scalable production system. The resulting GRP-enriched EVs retain functional activity exerting anti-inflammatory and calcification-inhibitory effects in human cell models, specifically in macrophages and primary VSMCs. Altogether, this work establishes a versatile platform for the production and delivery of bioactive GRP and paves the way for extending this approach to other VKDPs with therapeutic potential in chronic inflammatory and vascular disorders.

The bioengineering of VKDPs for research and therapeutic purposes has gained increasing interest, but remains a challenging task, particularly due to the requirement for γ-carboxylation to achieve fully bioactivity [16,17]. While major advantages of mammalian expression systems rely on endogenous carboxylation machinery, they are limited by low protein yields and incomplete γ-carboxylation, hampering their suitability for scalable production of fully active VKDPs [19–22]. In contrast, the BEVS offers high protein yields, scalability, and is easily adaptable to express multiple targets, while also supporting many mammalian-like post-translational modifications [23–26]. However, its potential to produce VKDPs remains controversial, largely due to contradictory findings on the presence and activity of key γ-carboxylation components, namely GGCX and VKOR. In this study, we demonstrate that cGRP can be successfully produced in vitamin K–supplemented Hi5 cells using BEVS, but only when GGCX and VKOR are co-expressed, indicating that Hi5 cells alone are insufficient to support GRP γ-carboxylation. This supports previous findings reporting low or absent endogenous carboxylation activity in insect cell lines such as Sf9 or Drosophila S2 [32–34], although other studies have suggested the presence of endogenous and potentially functional GGCX in S2 cells [27–31]. Notably, efforts to improve γ-carboxylation efficiency in both mammalian and BEVS platforms have relied on co-expression of GGCX alone or in combination with VKOR [19–22,32,34]. While GGCX is clearly essential for γ-carboxylation, the specific contribution of VKOR remains less well defined. In mammalian cells, VKOR has been identified as a potential rate-limiting step [19,21,54], whereas in BEVS, it appears to act synergistically with GGCX to enhance VKDP activity [32]. Although we did not evaluate the individual role of VKOR in our system, as it was always co-expressed with GGCX, our results confirm that their combined expression supports efficient GRP γ-carboxylation in BEVS. Also, our results demonstrate that vitamin K supplementation was indispensable for effective γ-carboxylation, as previous reported in both mammalian and insect cell systems [20,32].

In addition to the γ-carboxylation machinery, most VKDPs such as GRP, require cleavage of their propeptide for full posttranslational processing and efficient secretion of the mature protein [1,2,22]. In mammalian systems, limited proteolytic cleavage capacity by the endogenous proprotein convertase Furin has been associated to intracellular accumulation of unprocessed forms, ultimately reducing secretion yield. Co-expression of Furin has been shown to enhance propeptide cleavage and improve secretion efficiency [17,22]. Although insect cells are known to express endogenous Furin-like enzymes, their substrate specificity differs from mammalian Furin, sometimes resulting in incomplete processing of mammalian propeptides [55,56]. In the specific case of human VKDPs, substrate specificity and cleavage efficiency of insect Furin-like proteases remains uncharacterized. In our system, we observed that co-expression of human Furin was required to ensure proper GRP processing, suggesting that endogenous insect cell convertases are insufficient for complete maturation of mammalian VKDPs. Specifically, in the absence of exogenous Furin, or when Furin expression was low, the secreted GRP remained partially processed, as evidenced by Western blot and MS/MS analysis. Efficient propeptide cleavage and secretion of fully processed GRP was only achieved when high levels of human Furin were co-expressed, highlighting the need for robust Furin activity to support accurate post-translational maturation in BEVS.

Importantly, our findings demonstrate, for the first time, that GRP can be carried by EVs produced using the BEVS, and that these vesicles retain bioactivity in human recipient cells. While the BEVS is widely used in the biotechnological industry, particularly for the production of virus-like particles and subunit vaccines [25,57], its application to generate bioengineered EVs loaded with functional human proteins is still emerging [58]. Although EV secretion by *Spodoptera frugiperda* and *Trichoplusia ni* cells has been reported [58–60], their detailed characterization remains in early stages. EV isolation, characterization, and functional studies were performed in alignment with MISEV2018/2023 recommendations [51,53], serving as methodological guidelines where technically applicable. However, because insect-derived vesicles remain poorly characterized and specific molecular tools, such as antibodies recognizing insect EV markers, are largely unavailable, some criteria could only be addressed indirectly through complementary proteomic analysis.

Our combined approach for physical, morphological and molecular characterization for the different EVs populations isolated from the different systems demonstrated that BEVS-derived EVs share features with mammalian EVs, such as the size range, typical morphology and the presence of known EV markers. Of note, it is likely that additional EV markers have remained unidentified since the *Trichoplusia ni* proteome is not yet fully annotated, and protein identification relied mainly on homology with human counterparts. A few AcMNPV-derived proteins were also detected in all EV preparations. Although we cannot completely rule out residual contamination by budded virus particles, since no full separation was performed, previous studies have demonstrated that viral proteins can indeed associate with BEVS-derived vesicles [60].

Our isolation approach using sequential 30 K and 100 K centrifugal forces aimed to reduce the complexity and heterogeneity of EVs preparations, potentially enriching for larger and smaller vesicle subpopulations [39,50–52]. While no clear physical or morphological differences could be specifically associated to 30 K and 100 K EVs, proteomic profiling revealed distinct proteomes and differential expression patterns, suggesting underlying molecular differences. Importantly, both populations consistently contained canonical EV markers, including proteins commonly associated with small EVs such as CD63, SDCBP, PDCD6IP, TSG101 and ADAM10, reinforcing their vesicular identity [50,52]. Although we cannot at this stage infer on potential biogenesis differences between 30 K and 100 K, these results are consistent with previous reports describing the recovery of EVs with small EV-like features at centrifugal forces lower than the conventional 100 K [61]. Interestingly, we previously reported similar findings in EVs isolated from human primary VSMCs using a similar approach, further supporting that these subpopulations may share conserved molecular features with human EVs [39]. These results are also consistent with the well-recognized heterogeneity of EV subpopulations widely described in mammalian systems and underscore the need for deeper characterization to clarify their specific features and potential functional differences. Notably, our data revealed that GRP, together with the overexpressed human proteins GGCX, VKOR, and Furin, was consistently and preferentially enriched in the 30 K EVs, suggesting selective sorting into this subpopulation rather than a random distribution. The detection of GGCX and VKOR further indicates that, under conditions of recombinant protein overexpression, these key components of the vitamin K–dependent γ-carboxylation machinery can be associated with BEVS-derived EV populations. Although the present analysis is limited to MS/MS-based protein identification and does not address enzymatic activity, this observation is of particular interest given the central role of these enzymes in the post-translational modification of VKDPs and their broad physiological relevance [62,63]. In addition, the presence of Furin suggests that EVs may also incorporate this enzyme that is a key component of the maturation machinery required for the functional generation of most VKDPs. Together, these findings raise the possibility that EVs derived from BEVS may carry not only recombinant cargo proteins but also co-expressed components of their associated processing pathways, warranting further investigation to determine the functional

relevance of these associations.

Considering that γ-carboxylation has been shown to play a key role in the anti-calcifying activity of GRP [3–6], while both carboxylated and undercarboxylated forms have been implicated in the modulation of inflammatory responses [4,6–8], we performed a parallel evaluation of EV-associated GRP forms representing distinct γ-carboxylation states and potentially different biological activities relevant to calcification and inflammation control. Both cGRP- and ucGRP-EVs from the 30 K and 100 K fractions effectively interacted with THP-1–derived macrophages and VSMCs. While definitive internalization was not established, Western blot, flow cytometry and fluorescence microscopy indicate a clear association of EVs with recipient cells, suggesting that the observed functional effects are GRP-mediated, as GRP-free EVs displayed no detectable activity. These findings suggest that the biological effects observed are attributable to GRP cargo rather than nonspecific vesicle–cell interactions. Using a wide range of particles concentrations, we did not observe relevant decreased cell viability up to $7.5 \times 10^9$ or $1 \times 10^9$ particles/mL in THP-1 macrophages and VSMCs, respectively. This is consistent with the well-recognized biocompatibility of EVs and further supports the safety of vesicles produced in heterologous insect-cell systems. Importantly, the absence of cytotoxic effects also indicates that the presence of residual baculoviral proteins, which were detected in proteomic analyses and are likely integrated into the vesicular structures [60], does not compromise cell viability. This observation aligns with previous reports showing that baculoviruses and their components are non-replicative and non-toxic in mammalian cells [64,65]. However, at the highest concentration tested ($7.5 \times 10^9$ particles/mL), 100 K EVs elicited an immunological response, evidenced by elevated TNF-α release. Given the comparable dose–response patterns observed for 30 K and 100 K EVs at lower concentrations, it is plausible that a similar pro-inflammatory effect might also occur with 30 K EVs if tested at equivalent particle levels. However, this was not assessed due to the overall lower particle yields obtained for the 30 K fractions across all production systems. This response at high doses likely reflects a non-specific overload of the endocytic machinery rather than an intrinsic pro-inflammatory activity of BEVS-derived EVs, consistent with the notion that supraphysiological EV concentrations may trigger cellular stress, whereas more physiologically relevant, lower doses support controlled and functional EV-mediated signalling [66]. Notably, the higher GRP-to-EV ratio in 30 K vesicles may allow functional effects to be achieved with fewer particles, potentially reducing non-specific inflammatory responses.

The therapeutic potential of GRP-loaded vesicles as bioactive nanocarriers was assessed by their ability to modulate inflammation and calcification in macrophages and VSMCs. To ensure comparability across preparations, vesicle treatments were normalized to GRP content, allowing a GRP dose-dependent evaluation of biological effects. Remarkably, both cGRP- and ucGRP-EVs showed anti-inflammatory and anti-calcifying activities. Consistent with previous reports, GRP anti-inflammatory effects appear largely independent of γ-carboxylation [4,6–8], whereas calcification inhibition is structurally and functionally more dependent on γ-carboxylation due to its role in calcium binding and mineral interaction [3–6]. Accordingly, cGRP-EVs consistently produced stronger reduction of VSMC calcification across all tested concentrations supporting the biological relevance of γ-carboxylation in modulating mineral deposition. In contrast, ucGRP-EVs also decreased calcification, albeit to a lesser extent, but displayed increased anti-inflammatory activity in this calcification-related context. This suggests that ucGRP-EVs may partially modulate calcification indirectly through inflammatory pathways. Additionally, ucGRP has been previously detected at sites of pathological calcification [1,3,67], and its negatively charged glutamic acid residues may confer a limited intrinsic capacity to inhibit mineral deposition, as described for other calcification inhibitors [68]. Furthermore, the effects of ucGRP-EVs likely reflect not only ucGRP itself but also the broader composition of the vesicles, which may contribute synergistically to their bioactivity.

Although all EV populations were normalized to GRP content, a consistently stronger anti-inflammatory effect in THP-1 macrophages was observed with 100 K EVs compared to 30 K EVs, independent of GRP γ-carboxylation status. Because no preferential uptake of either vesicle type was detected, these differences are unlikely to reflect GRP dose or delivery efficiency. Instead, they may arise from intrinsic molecular distinctions between the vesicle subpopulations, as supported by their distinct proteomic profiles, suggesting that compositional features specific to 100 K EVs may potentiate GRP-associated signalling effects.

While the present study focused on establishing BEVS as a platform for EV-mediated delivery of γ-carboxylated GRP, addressing known limitations related to solubility, formulation, and protein bioavailability, direct functional comparison with free GRP in the same cellular models was not performed, and in vivo validation remains to be addressed. These aspects are acknowledged as limitations. Nevertheless, the data demonstrate that GRP retains functional biological activity when incorporated into EV-based delivery systems at markedly lower concentrations than previously reported for the free protein [3,7], reinforcing the importance of γ-carboxylation for optimizing its anti-calcific properties and underscoring the added value of BEVS in enabling the production of mature cGRP with translational potential.

## 5. Conclusions

In conclusion, this work establishes a baculovirus/insect-cell platform capable of producing γ-carboxylated GRP and simultaneously association with secreted extracellular vesicles with preserved biological functionality. The resulting GRP-enriched EVs display dual anti-inflammatory and anti-calcifying properties in human macrophage and vascular smooth muscle cell models, confirming the retention of GRP activity in EVs. Importantly, the vesicle formulations showed no cytotoxicity, supporting their safety and biocompatibility despite their insect cell origin. These findings not only demonstrate the feasibility of BEVS for scalable production of functional VKDPs but also position GRP-EVs as promising bioinspired nanocarriers for the modulation of inflammation and vascular calcification. This strategy may be broadly applicable to other vitamin K–dependent proteins, paving the way for new therapeutic avenues in chronic inflammatory and cardiovascular disorders.

## CRediT authorship contribution statement

**Carla Viegas:** Writing – review & editing, Writing – original draft, Visualization, Validation, Supervision, Project administration, Methodology, Investigation, Funding acquisition, Formal analysis, Data curation, Conceptualization. **Simon Pichard:** Writing – review & editing, Visualization, Validation, Investigation, Formal analysis, Data curation. **Joana Carreira:** Writing – review & editing, Visualization, Validation, Investigation, Formal analysis, Data curation. **Adélia Ova:** Writing – review & editing, Validation, Investigation, Data curation. **Nathalie Troffer-Charlier:** Writing – review & editing, Investigation, Data curation. **Teresa M. Maia:** Writing – review & editing, Visualization, Investigation, Formal analysis, Data curation. **Evelina Edelweiss:** Writing – review & editing, Investigation. **Anjos L. Macedo:** Writing – review & editing, Visualization, Investigation, Data curation. **António Matos:** Writing – review & editing, Visualization, Investigation. **Tiago Q. Faria:** Writing – review & editing, Visualization, Investigation, Formal analysis, Data curation. **Sofia M. Calado:** Writing – review & editing, Visualization, Validation, Investigation, Formal analysis. **Carina Monico:** Writing – review & editing, Visualization, Investigation, Formal analysis. **Simon Devos:** Writing – review & editing, Supervision, Project administration. **Francis Impens:** Writing – review & editing, Supervision, Project administration. **Christine Schaeffer-Reiss:** Writing – review & editing, Investigation. **Sarah Cianférani:** Writing – review & editing, Investigation. **Cristina Peixoto:** Writing – review & editing, Investigation. **Arnaud Poterszman:** Writing – review & editing,

Writing – original draft, Visualization, Validation, Supervision, Project administration, Methodology, Investigation, Data curation, Conceptualization. **Dina Simes:** Writing – review & editing, Supervision, Funding acquisition, Conceptualization.

## Declaration of competing interest

Carla Viegas and Dina Simes are co-founders of GenoGla Diagnostics. A PCT patent application PCT/PT2009000046, is owned by the University of Algarve and the Centre of Marine Sciences (CCMAR), and the exclusive rights are licensed to GenoGla Diagnostics. The remaining authors declare no financial or non-financial competing interests. The disclosed interests did not influence the design, execution, or interpretation of the study.

## Acknowledgements (with funding)

This research was funded by Portuguese National Funds from FCT—Foundation for Science and Technology, through the PhD grant 2022.12777.BD, project EXPL/BTM-TEC/0990/2021, contracts UID/04326/2025, UID/PRR/04326/2025 and LA/P/0101/2020 (DOI:10.54499/LA/P/0101/2020), from the operational programmes CRESC Algarve 2020 and COMPETE 2020 through contract EMBRC.PT ALG-01-0145-FEDER-02 and MarPlus project, by transnational accesses provided by the European Proteomics Infrastructure Consortium—Providing Access (EPIC-XS2019 project #7) and by the Portuguese Society of Nephrology (SPN) through projects funding. This work benefited from access to the resources of the French Infrastructure for Integrated Structural Biology (FRISBI) (ANR-10-INBS-0005) and of Instruct-ERIC (EU project PID7060), along with the French Proteomic Infrastructure (ProFI) project (ANR-10-INBS-08 and ANR-24-INBS-0015) are acknowledged.

The authors thank Leon Schurgers, Department of Biochemistry, CARIM, Maastricht University, The Netherlands, for providing the primary VSMC cultures used in this study; and to Sara Nascimento, iBET and ITQB-NOVA for supporting in NTA assay.

## Appendix A. Supplementary data

Supplementary data to this article can be found online at https://doi.org/10.1016/j.bioadv.2026.214833.

## Data availability

All data needed to evaluate the conclusions in the paper are present in the paper and/or the Supplementary Materials. Additional data related to this paper may be requested from the authors.

## References

[1] C.S. Viegas, D.C. Simes, V. Laizé, M.K. Williamson, P.A. Price, M.L. Cancela, Gla-rich protein (GRP), a new vitamin K-dependent protein identified from sturgeon cartilage and highly conserved in vertebrates, J. Biol. Chem. 283 (2008) 36655–36664, https://doi.org/10.1074/jbc.M802761200.

[2] C. Surmann-Schmitt, U. Dietz, T. Kireva, N. Adam, J. Park, A. Tagariello, P. Onnerfjord, D. Heinegård, U. Schlötzer-Schrehardt, R. Deutzmann, et al., Ucma, a novel secreted cartilage-specific protein with implications in osteogenesis, J. Biol. Chem. 283 (2008) 7082–7093, https://doi.org/10.1074/jbc.M702792200.

[3] C.S. Viegas, M.S. Rafael, J.L. Enriquez, A. Teixeira, R. Vitorino, I.M. Luís, R. M. Costa, S. Santos, S. Cavaco, J. Neves, A.L. Macedo, B.A. Willems, C. Vermeer, D. C. Simes, Gla-rich protein acts as a calcification inhibitor in the human cardiovascular system, Arterioscler. Thromb. Vasc. Biol. 35 (2015) 399–408, https://doi.org/10.1161/ATVBAHA.114.304823.

[4] C.S.B. Viegas, L. Santos, A.L. Macedo, A.A. Matos, A.P. Silva, P.L. Neves, A. Staes, K. Gevaert, R. Morais, C. Vermeer, et al., Chronic Kidney Disease circulating calciprotein particles and extracellular vesicles promote vascular calcification: a role for GRP (Gla-rich protein), Arterioscler. Thromb. Vasc. Biol. 38 (2018) 575–587, https://doi.org/10.1161/atvbaha.117.310578.

[5] B.A. Willems, M. Furmanik, M.M.J. Caron, M.L.L. Chatrou, D.H.M. Kusters, T.J. M. Welting, M. Stock, M.S. Rafael, C.S.B. Viegas, D.C. Simes, et al., Ucma/GRP inhibits phosphate-induced vascular smooth muscle cell calcification via SMAD-dependent BMP signalling, Sci. Rep. 8 (2018) 4961, https://doi.org/10.1038/s41598-018-23353-y.

[6] S. Cavaco, C.S. Viegas, M.S. Rafael, A. Ramos, J. Magalhães, F.J. Blanco, C. Vermeer, D.C. Simes, Gla-rich protein is involved in the cross-talk between calcification and inflammation in osteoarthritis, Cell. Mol. Life Sci. 73 (2016) 1051–1065, https://doi.org/10.1007/s00018-015-2033-9.

[7] C.S.B. Viegas, R.M. Costa, L. Santos, P.A. Videira, Z. Silva, N. Araújo, A.L. Macedo, A.P. Matos, C. Vermeer, D.C. Simes, Gla-rich protein functions as an anti-inflammatory agent in monocytes/macrophages: implications for calcification-related chronic inflammatory diseases, PloS One 12 (2017) e0177829, https://doi.org/10.1371/journal.pone.0177829.

[8] C.S.B. Viegas, N. Araújo, J. Carreira, J.F. Pontes, A.L. Macedo, M. Vinhas, A. S. Moreira, T.Q. Faria, A. Grenha, A.A. de Matos, L. Schurgers, C. Vermeer, D. C. Simes, Nanoencapsulation of Gla-rich protein (GRP) as a novel approach to target inflammation, Int. J. Mol. Sci. 23 (2022) 4813, https://doi.org/10.3390/ijms23094813.

[9] M. Stock, S. Menges, N. Eitzinger, M. Geßlein, R. Botschner, L. Wormser, A. Distler, U. Schlötzer-Schrehardt, K. Dietel, J. Distler, C. Beyer, K. Gelse, K. Engelke, M. I. Koenders, W. van den Berg, K. von der Mark, G. Schett, A dual role of upper zone of growth plate and cartilage matrix-associated protein in human and mouse osteoarthritic cartilage: inhibition of aggrecanases and promotion of bone turnover, Arthritis Rheumatol. 69 (2017) 1233–1245, https://doi.org/10.1002/art.40042.

[10] F. Seuffert, D. Weidner, W. Baum, G. Schett, M. Stock, Upper zone of growth plate and cartilage matrix-associated protein protects cartilage during inflammatory arthritis, Arthritis Res. Ther. 20 (2018) 88, https://doi.org/10.1186/s13075-018-1583-2.

[11] A.P. Silva, C.S. Viegas, F. Mendes, A. Macedo, P. Guilherme, N. Tavares, C. Dias, F. Rato, N. Santos, M. Faísca, et al., Gla-rich protein (GRP) as an early and novel marker of vascular calcification and kidney dysfunction in diabetic patients with CKD: a pilot cross-sectional study, J. Clin. Med. 9 (2020) 635, https://doi.org/10.3390/jcm9030635.

[12] A.P. Silva, C.S.B. Viegas, P. Guilherme, N. Tavares, C. Dias, F. Rato, N. Santos, M. Faísca, E. de Almeida, P.L. Neves, et al., Gla-rich protein, magnesium and phosphate associate with mitral and aortic valves calcification in diabetic patients with moderate CKD, Diagnostics 12 (2022) 496, https://doi.org/10.3390/diagnostics12020496.

[13] C. Marreiros, C. Viegas, A.P. Silva, M. Faísca, L. Schurgers, D. Simes, Gla-rich protein is associated with vascular calcification, inflammation and mineral markers in peritoneal dialysis patients, J. Clin. Med. 13 (2024) 7429, https://doi.org/10.3390/jcm13237429.

[14] J.K. Tie, D.W. Stafford, Structural and functional insights into enzymes of the vitamin K cycle, J. Thromb. Haemost. 14 (2016) 236–247, https://doi.org/10.1111/jth.13217.

[15] K.L. Berkner, K.W. Runge, Vitamin K-dependent protein activation: normal γ-glutamyl carboxylation and disruption in disease, Int. J. Mol. Sci. 23 (2022) 5759, https://doi.org/10.3390/ijms23105759.

[16] K.L. Berkner, Expression of recombinant vitamin K-dependent proteins in mammalian cells: factors IX and VII, Methods Enzymol. 222 (1993) 450–477, https://doi.org/10.1016/0076-6879(93)22029-F.

[17] S.R. Kumar, Industrial production of clotting factors: challenges of expression and choice of host cells, Biotechnol. J. 10 (2015) 995–1004, https://doi.org/10.1002/biot.201400666.

[18] R.M. Camire, P.J. Larson, D.W. Stafford, K.A. High, Enhanced γ-carboxylation of recombinant factor X using a chimeric construct containing the prothrombin propeptide, Biochemistry 39 (2000) 14322–14329, https://doi.org/10.1021/bi001074q.

[19] N. Wajih, D.C. Sane, S.M. Hutson, R. Wallin, Engineering of a recombinant vitamin K-dependent γ-carboxylation system with enhanced γ-carboxyglutamic acid–forming capacity: evidence for a functional CXXC redox center, J. Biol. Chem. 280 (2005) 10540–10547, https://doi.org/10.1074/jbc.M413982200.

[20] K.W. Hallgren, E.L. Hommema, B.A. McNally, K.L. Berkner, Carboxylase overexpression effects full carboxylation but poor release and secretion of factor IX: implications for release of vitamin K-dependent proteins, Biochemistry 41 (2002) 15045–15055, https://doi.org/10.1021/bi026016e.

[21] N. Wajih, S.M. Hutson, J. Owen, R. Wallin, Increased production of functional recombinant human clotting factor IX by BHK cells engineered to overexpress VKORC1, J. Biol. Chem. 280 (2005) 31603–31607, https://doi.org/10.1074/jbc.M505373200.

[22] J. Liu, A. Jonebring, J. Hagström, A.C. Nyström, A. Lövgren, Improved expression of recombinant human factor IX by co-expression of GGCX, VKOR and furin, Protein J. 33 (2014) 174–183, https://doi.org/10.1007/s10930-014-9550-5.

[23] J. Osz-Papai, L. Radu, W. Abdulrahman, I. Kolb-Cheynel, N. Troffer-Charlier, C. Birck, A. Poterszman, Insect cells–baculovirus system for the production of difficult-to-express proteins, Methods Mol. Biol. 1258 (2015) 181–205, https://doi.org/10.1007/978-1-4939-2205-5_10.

[24] M. Hong, T. Li, W. Xue, S. Zhang, L. Cui, H. Wang, Y. Zhang, L. Zhou, Y. Gu, N. Xia, S. Li, Genetic engineering of baculovirus–insect cell system to improve protein production, Front. Bioeng. Biotechnol. 10 (2022) 994743, https://doi.org/10.3389/fbioe.2022.994743.

[25] A.M. Targovnik, J.A. Simonin, G.J. Mc Callum, I. Smith, F.U. Cuccovia Warlet, M. V. Nugnes, M.V. Miranda, M.N. Belaich, Solutions against emerging human diseases through baculovirus technologies, Appl. Microbiol. Biotechnol. 105 (2021) 8195–8226, https://doi.org/10.1007/s00253-021-11615-1.

[26] I. Berger, A. Poterszman, Baculovirus expression: old dog, new tricks, Bioengineered 6 (2015) 316–322, https://doi.org/10.1080/21655979.2015.1104433.
[27] T. Li, C.T. Yang, D. Jin, D.W. Stafford, Identification of a Drosophila vitamin K-dependent γ-glutamyl carboxylase, J. Biol. Chem. 275 (2000) 18291–18296, https://doi.org/10.1074/jbc.M001790200.
[28] P.K. Bandyopadhyay, K. Clark, B.J. Stevenson, J.E. Rivier, B.M. Olivera, K.G. Golic, Y.S. Rong, Biochemical characterization of Drosophila γ-glutamyl carboxylase and its role in fly development, Insect Mol. Biol. 15 (2006) 147–156, https://doi.org/10.1111/j.1365-2583.2006.00619.x.
[29] H.M. Robertson, Genes encoding vitamin K epoxide reductase are present in Drosophila and trypanosomatid protists, Genetics 168 (2004) 1077–1080, https://doi.org/10.1534/genetics.104.029744.
[30] J. Vatandoost, A. Zomorodipour, M. Sadeghizadeh, R. Aliyari, M.H. Bos, F. Ataei, Expression of biologically active human clotting factor IX in Drosophila S2 cells: γ-carboxylation by the insect enzyme, Biotechnol. Prog. 28 (2012) 45–51, https://doi.org/10.1002/btpr.723.
[31] J. Vatandoost, M.H. Bos, Efficient expression of functional human coagulation factor IX in stably transfected Drosophila S2 cells: comparison with CHO system, Biotechnol. Lett. 38 (2016) 1691–1698, https://doi.org/10.1007/s10529-016-2156-6.
[32] K. Nagahashi, K. Umemura, N. Kanayama, T. Iwaki, Successful synthesis of active human coagulation factor VII in Drosophila S2 cells by co-expression of mammalian γ-glutamyl carboxylase and vitamin K cycle modification, Cytotechnology 69 (2017) 317–327, https://doi.org/10.1007/s10616-016-0059-y.
[33] D.A. Roth, A. Rehemtulla, R.J. Kaufman, C.T. Walsh, B. Furie, B.C. Furie, Expression of bovine vitamin K-dependent carboxylase activity in baculovirus-infected insect cells, Proc. Natl. Acad. Sci. U. S. A. 90 (1993) 8372–8376, https://doi.org/10.1073/pnas.90.18.8372.
[34] N. Masroori, R. Halabian, M. Mohammadipour, A.M. Roushandeh, M. Rouhbakhsh, A.J. Najafabadi, M.E. Fathabad, M. Salimi, M.A. Shokrgozar, M.H. Roudkenar, High-level expression of functional recombinant human coagulation factor VII in insect cells, Biotechnol. Lett. 32 (2010) 803–809, https://doi.org/10.1007/s10529-010-0227-7.
[35] Y.J. Liu, C. Wang, A review of the regulatory mechanisms of extracellular vesicles-mediated intercellular communication, Cell Commun. Signal 21 (2023) 77, https://doi.org/10.1186/s12964-023-01103-6.
[36] Q. Liu, D. Li, X. Pan, Y. Liang, Targeted therapy using engineered extracellular vesicles: principles and strategies for membrane modification, J. Nanobiotechnol. 21 (2023) 334, https://doi.org/10.1186/s12951-023-02081-0.
[37] S. Du, Y. Guan, A. Xie, Z. Yan, S. Gao, W. Li, L. Rao, X. Chen, T. Chen, Extracellular vesicles: a rising star for therapeutics and drug delivery, J. Nanobiotechnol. 21 (2023) 231, https://doi.org/10.1186/s12951-023-01973-5.
[38] X. Lu, S. Fan, M. Cao, et al., Extracellular vesicles as drug delivery systems in therapeutics: current strategies and future challenges, J. Pharm. Investig. 54 (2024) 785–802, https://doi.org/10.1007/s40005-024-00699-2.
[39] C. Viegas, J. Carreira, T.M. Maia, A.L. Macedo, A.P. Matos, J. Neves, D. Simes, Gla-rich protein mediates vascular smooth muscle cell osteogenic differentiation, extracellular vesicle calcification propensity and immunomodulatory properties, Int. J. Mol. Sci. 25 (2024) 12406, https://doi.org/10.3390/ijms252212406.
[40] O. Kolesnikova, A. Zachayus, S. Pichard, J. Osz, N. Rochel, P. Rossolillo, I. Kolb-Cheynel, N. Troffer-Charlier, E. Compe, O. Bensaude, I. Berger, A. Poterszman, HR-Bac, a toolbox based on homologous recombination for expression, screening and production of multiprotein complexes using the baculovirus expression system, Sci. Rep. 12 (2022) 2030, https://doi.org/10.1038/s41598-021-04715-5.
[41] I. Berger, D.J. Fitzgerald, T.J. Richmond, Baculovirus expression system for heterologous multiprotein complexes, Nat. Biotechnol. 22 (2004) 1583–1587, https://doi.org/10.1038/nbt1036.
[42] C. Chiva, R. Olivella, E. Borràs, G. Espadas, O. Pastor, A. Solé, E. Sabidó, QCloud: a cloud-based quality control system for mass spectrometry-based proteomics laboratories, PLoS One 13 (2018) e0189209, https://doi.org/10.1371/journal.pone.0189209.
[43] R. Olivella, C. Chiva, M. Serret, D. Mancera, L. Cozzuto, A. Hermoso, E. Borràs, G. Espadas, J. Morales, O. Pastor, A. Solé, J. Ponomarenko, E. Sabidó, QCloud2: an improved cloud-based quality-control system for mass-spectrometry-based proteomics laboratories, J. Proteome Res. 20 (2021) 2010–2013, https://doi.org/10.1021/acs.jproteome.0c00853.
[44] Z. Ning, D. Seebun, B. Hawley, C.K. Chiang, D. Figeys, From cells to peptides: "one-stop" integrated proteomic processing using amphipols, J. Proteome Res. 12 (2013) 1512–1519, https://doi.org/10.1021/pr301064z.
[45] C. Camacho, G. Coulouris, V. Avagyan, N. Ma, J. Papadopoulos, K. Bealer, T. L. Madden, BLAST+: architecture and applications, BMC Bioinform. 10 (2009) 421, https://doi.org/10.1186/1471-2105-10-421.
[46] J.L. Reynolds, A.J. Joannides, J.N. Skepper, R. McNair, L.J. Schurgers, D. Proudfoot, W. Jahnen-Dechent, P.L. Weissberg, C.M. Shanahan, Human vascular smooth muscle cells undergo vesicle-mediated calcification in response to changes in extracellular calcium and phosphate concentrations: a potential mechanism for accelerated vascular calcification in ESRD, J. Am. Soc. Nephrol. 15 (2004) 2857–2867, https://doi.org/10.1097/01.ASN.0000141960.01035.28.
[47] T. Duellman, J. Burnett, J. Yang, Quantitation of secreted proteins using mCherry fusion constructs and a fluorescent microplate reader, Anal. Biochem. 473 (2015) 34–40, https://doi.org/10.1016/j.ab.2014.12.010.
[48] D. Ershov, M.S. Phan, J.W. Pylvänäinen, S.U. Rigaud, L. Le Blanc, A. Charles-Orszag, J.R.W. Conway, R.F. Laine, N.H. Roy, D. Bonazzi, G. Duménil, G. Jacquemet, J.Y. Tinevez, TrackMate 7: integrating state-of-the-art segmentation algorithms into tracking pipelines, Nat. Methods 19 (2022) 829–832, https://doi.org/10.1038/s41592-022-01507-1.
[49] C.S. Viegas, S. Cavaco, P.L. Neves, A. Ferreira, A. João, M.K. Williamson, P. A. Price, M.L. Cancela, D.C. Simes, Gla-rich protein is a novel vitamin K-dependent protein present in serum that accumulates at sites of pathological calcifications, Am. J. Pathol. 175 (2009) 2288–2298, https://doi.org/10.2353/ajpath.2009.090474.
[50] A. Lischnig, M. Bergqvist, T. Ochiya, C. Lässer, Quantitative proteomics identifies proteins enriched in large and small extracellular vesicles, Mol. Cell. Proteomics 21 (2022) 100273, https://doi.org/10.1016/j.mcpro.2022.100273.
[51] C. Théry, K.W. Witwer, E. Aikawa, et al., Minimal information for studies of extracellular vesicles 2018 (MISEV2018): a position statement of the International Society for Extracellular Vesicles and update of the MISEV2014 guidelines, J. Extracell. Vesicles 7 (2018) 1535750, https://doi.org/10.1080/20013078.2018.1535750.
[52] J. Kowal, G. Arras, M. Colombo, M. Jouve, J.P. Morath, B. Primdal-Bengtson, F. Dingli, D. Loew, M. Tkach, C. Théry, Proteomic comparison defines novel markers to characterize heterogeneous populations of extracellular vesicle subtypes, Proc. Natl. Acad. Sci. U. S. A. 113 (2016) E968–E977, https://doi.org/10.1073/pnas.1521230113.
[53] J.A. Welsh, D.C.I. Goberdhan, L. O'Driscoll, et al., Minimal information for studies of extracellular vesicles (MISEV2023): from basic to advanced approaches, J. Extracell. Vesicles 13 (2024) e12404, https://doi.org/10.1002/jev2.12404.
[54] S.F. Pakdaman, J. Vatandoost, M.H.A. Bos, Enhanced functional recombinant factor IX production by human embryonic kidney cells engineered to overexpress VKORC1, Biotechnol. Prog. 36 (2020) e2938, https://doi.org/10.1002/btpr.2938.
[55] G.L. Cano-Monreal, J.C. Williams, H.W. Heidner, An arthropod enzyme, Dfurin1, and a vertebrate furin homolog display distinct cleavage-site sequence preferences for a shared viral proprotein substrate, J. Insect Sci. 10 (2010) 29, https://doi.org/10.1673/031.010.2901.
[56] H. Posthaus, C.M. Dubois, M.H. Laprise, F. Grondin, M.M. Suter, E. Müller, Proprotein cleavage of E-cadherin by furin in baculovirus over-expression system: potential role of other convertases in mammalian cells, FEBS Lett. 438 (1998) 306–310, https://doi.org/10.1016/S0014-5793(98)01330-1.
[57] J.H. Tian, N. Patel, R. Haupt, H. Zhou, S. Weston, H. Hammond, J. Logue, A. D. Portnoff, J. Norton, M. Guebre-Xabier, B. Zhou, K. Jacobson, S. Moffitt, W. Kluepfel-Stahl, S. Ekechukwu, B. Papin, S. Boddapati, C. Jason Wong, P. A. Piedra, M.B. Frieman, M.J. Massare, L. Fries, K.L. Bengtsson, Immunogenicity in baboons and protection in mice of SARS-CoV-2 spike glycoprotein vaccine candidate NVX-CoV2373, Nat. Commun. 12 (2021) 372, https://doi.org/10.1038/s41467-020-20653-8.
[58] R. Ishikawa, S. Yoshida, S.I. Sawada, Y. Sasaki, K. Akiyoshi, Preparation of engineered extracellular vesicles with full-length functional PD-1 membrane proteins by baculovirus expression system, Biochem. Biophys. Res. Commun. 526 (2020) 967–972, https://doi.org/10.1016/j.bbrc.2020.03.187.
[59] C.S. Hausjell, W. Ernst, C. Grünwald-Gruber, E. Arcalis, R. Grabherr, Quantitative proteomic analysis of extracellular vesicles in response to baculovirus infection of a Trichoplusia ni cell line, PloS One 18 (2023) e0281060, https://doi.org/10.1371/journal.pone.0281060.
[60] L.J.C. van Es, R.D. Possee, L.A. King, Characterisation of extracellular vesicles in baculovirus infection of Spodoptera frugiperda cells, J. Extracell. Biol. 3 (2024) e163, https://doi.org/10.1002/jex2.163.
[61] D.K. Jeppesen, M.L. Hvam, B. Primdahl-Bengtson, A.T. Boysen, B. Whitehead, L. Dyrskjøt, T.F. Orntoft, K.A. Howard, M.S. Ostenfeld, Comparative analysis of discrete exosome fractions obtained by differential centrifugation, J. Extracell. Vesicles 3 (2014) 25011, https://doi.org/10.3402/jev.v3.25011.
[62] D.C. Simes, C.S.B. Viegas, N. Araújo, C. Marreiros, Vitamin K as a powerful micronutrient in aging and age-related diseases: pros and cons from clinical studies, Int. J. Mol. Sci. 20 (2019) 4150, https://doi.org/10.3390/ijms20174150.
[63] D.C. Simes, C.S.B. Viegas, N. Araújo, C. Marreiros, Vitamin K as a diet supplement with impact in human health: current evidence in age-related diseases, Nutrients 12 (2020) 138, https://doi.org/10.3390/nu12010138.
[64] M.L. Pidre, P.N. Arrías, L.C. Amorós Morales, V. Romanowski, The magic staff: A comprehensive overview of baculovirus-based technologies applied to human and animal health, Viruses 15 (2022) 80, https://doi.org/10.3390/v15010080.
[65] S. Schaly, M. Ghebretatios, S. Prakash, Baculoviruses in gene therapy and personalized medicine, Biologics 15 (2021) 115–132, https://doi.org/10.2147/BTT.S292692.
[66] D.W. Hagey, M. Ojansivu, B.R. Bostancioglu, O. Saher, J.P. Bost, M.O. Gustafsson, R. Gramignoli, M. Svahn, D. Gupta, M.M. Stevens, A. Görgens, S. El Andaloussi, The cellular response to extracellular vesicles is dependent on their cell source and dose, Sci. Adv. 9 (2023) eadh1168, https://doi.org/10.1126/sciadv.adh1168.
[67] C.S. Viegas, M. Herfs, M.S. Rafael, J.L. Enriquez, A. Teixeira, I.M. Luís, C.M. van 't Hoofd, A. João, V.L. Maria, S. Cavaco, A. Ferreira, M. Serra, E. Theuwissen, C. Vermeer, D.C. Simes, Gla-rich protein is a potential new vitamin K target in cancer: evidences for a direct GRP-mineral interaction, Biomed. Res. Int. 2014 (2014) 340216, https://doi.org/10.1155/2014/340216.
[68] S.A. Steitz, M.Y. Speer, M.D. McKee, L. Liaw, M. Almeida, H. Yang, C.M. Giachelli, Osteopontin inhibits mineral deposition and promotes regression of ectopic calcification, Am. J. Pathol. 161 (2002) 2035–2046, https://doi.org/10.1016/S0002-9440(10)64482-3.